Calhoun: The NPS Institutional Archive

DSpace Repository

Theses and Dissertations 1. Thesis and Dissertation Collection, all items

1969

Bending of ferro-cement plates.

Claman, John S.

http://hdl.handle.net/10945/11731

Downloaded from NPS Archive: Calhoun

Calhoun is the Naval Postgraduate School's public access digital repository for research materials and institutional publications created by the NPS community. Calhoun is named for Professor of Mathematics Guy K. Calhoun, NPS's first appointed -- and published -- scholarly author.

Dudley Knox Library / Naval Postgraduate School
411 Dyer Road / 1 University Circle
Monterey, California USA 93943

http://www.nps.edu/library

NPS ARCHIVE
1969
CLAMAN, J.

BENDING OF FERRO-CEMENT PLATES

JOHN S. CLAMAN

NAV. ENG. N.A.M.E. JUNE 1969

RARY
L POSTGRADUATE SCHOOL
TEREY, CALIF. 93940

DUDLEY KNOX LIBRARY
NAVAL POSTGRADUATE SCHOOL
MONTEREY, CA 93943-5101

BENDING OF FERRO-CEMENT PLATES

By

LT. JOHN S. CLAMAN USN
//

SUBMITTED IN PARTIAL FULFILLMENT OF THE REQUIREMENTS
FOR THE DEGREE OF NAVAL ENGINEER AND THE DEGREE OF
MASTER OF SCIENCE IN MARINE ENGINEERING

at the

MASSACHUSETTS INSTITUTE OF TECHNOLOGY

May, 1969

NAVAL POSTGRADUATE SCHOOL
MONTEREY, CALIF. 93940

DUDLEY KNOX LIBRARY
NAVAL POSTGRADUATE SCHOOL
MONTEREY, CA 93943-5101

ABSTRACT

Title: Bending of Ferro-Cement Plates

Author: Lt. John S. Claman USN

Submitted to the Department of Naval Architecture and Marine Engineering on May 23, 1969 in partial fulfillment of the requirement for the degrees of Naval Engineer and Master of Science in Marine Engineering.

The experimental findings for bending of square ferro-cement plates under a central concentrated load using three types of reinforcement are compared to the predicted results of a finite element analysis based on the input of experimentally determined material properties. The material properties are obtained from tensile, flexural, compression, shear and impact tests. The variation of properties between the three types of reinforced mortar is correlated with the plate bending results and the theory of fiberous reinforced composites.

Thesis Supervisor: Frederic Moavenzadeh, Associate Professor of Civil Engineering, Massachusetts Institute of Technology

ACKNOWLEDGMENT

The author is greatly indebted to Professor Fred Moavenzadeh for his guidance and patience which made the writing of this thesis possible.

The author further wishes to thank Professor Jerome J. Conner Jr. for his help with the finite analysis program/

He is also especially indebted to his wife Joyce, for her tireless patience and typing skill.

CONTENTS

Page

Title Page 1

Abstract 2

Acknowledgement 3

Contents 4

List of Figures and Tables 6

I Introduction 8

II Theory 12

- A. Mechanism of Fracture in an Elasto-Plastic Material 12
- B. Mechanism of Fracture in Ferro-Cement 14
- C. Bending of Plates 18
  - 1. Orthotropic Constitutive Relations 19
  - 2. Elastic Plate Bending 21
  - 3. Plastic Plate Bending 27

III Experimental Procedure 35

- A. Plate Bending 35
- B. Material Properties 37

IV Experimental Results 44

V Discussion of Results 49

- A. Material Properties in x, y Direction
  - 1. Tensile Strength 49
  - 2. Modulus of Elasticity 53
- B. Material Properties 45° to x, y Direction 59
- C. Other Properties 60

Page
1. Shear Strength 60
2. Impact Energy 61
D. Cylinder Compression Tests 63
E. Plate Bending 66
F. Finite Element Analysis 70
VI Conclusions 80
VII Recommendations 82
VIII References 83
Appendix IA Experimental Results: Series A 88
IB Experimental Results: Series B 91
IC Experimental Results: Series C 94
ID Experimental Results: Cylinder Compression Tests 97
Appendix II Computer Program Input Output Data 99
Appendix III Classical Homogeneous Plate Bending Theory Prediction 101

LIST OF FIGURES AND TABLES

Table I Material Specifications

Table II Summary of Experimental Results

Figure 1. Crack Traversing Fiber Reinforced Matrix

2. Square Plate Loaded at Center

3. Stress-Strain Curve for Elasto Plastic Material

4. Incremental Elasto-Plastic Analysis Method Simple Tension

5. Method of Plate Loading

6. Flexure Test Apparatus

7. Tensile Test Apparatus

8. Shear Test Apparatus

9. Tensile Test Data x,y Axis

10. Tensile Test Data 45^0 to x, y Axis

11. Flexure Test Data x, y Axis

12. Flexure Test Data 45^0 to x, y Axis

13. Shear Stress and Impact Energy Data

14. Cylinder Compression Test Data: Stress Strain

15. Cylinder Compression Test Data: Modulus of Elasticity and Compressive Strength

16. Plate Bending: Normalized Load-Deflection of Center Point, Bending Region (All Series)

17. Plate Bending: Normalized Load-Deflection of Center Point, Membrane Region (All Series)

18. Plate Bending: Series "A" Load-Deflection of Center Point (Experimental and Finite Element Analysis)

19. Plate Bending: Series "B" Load-Deflection of Center Point

20. Plate Bending: Series "C" Load-Deflection of Center Point

21. Plate Bending: Normalized Plate Deflection Surface Along x Axis (All Series)

22. Compression Cylinders After Ultimate Failure

23. Plate Specimens After Ultimate Failure

24. Typical Load Deflection/Strain Curves for Tension Tests

I INTRODUCTION

During WWI and WWII the possibility of a shortage of steel plate caused the U.S. Government to contract for ships made from reinforced concrete (1). These ships were generally satisfactory for their purpose but were considered to be only temproary in nature because of the limited mechanical properties of the reinforced concrete when compared to the requirements for sturdy long lasting marine construction. Work originally performed by the Italian Architect P.L. Nervi and expanded by numerous investigators in the past two decades indicates that the structural requirements of marine construction can be approached in Portland cement concrete by the use of closely spaced wire mesh and/or chopped wire fiber as reinforcement. This material is commonly called "ferro-cement" and its use in marine construction has been increasing as evidenced by the number of boat builders from England to Communist China which are involved in constructing marine barges, trawlers and houseboats from the material. Ferro-cement has particular application in countries where steel is scarce and labor is an excess commodity

The important mechanical properties required of a material for marine construction are:

1) High tensile, compressive and shear strength.

2) High fracture toughness and impact resistance.

3) Low density.

4) Good fatigue and low creep characteristics.

5) High modulus of elasticity.

6) Deterministic and predictable mechanical properties.

The economic and durable properties required of marine structural materials are:

1) Low cost.

2) Easy to fabricate and handle.

3) Easy to repair.

4) Low maintenance requirement.

5) High resistance to corrosion, abrasion and attack from the marine environment .

6) Waterproof.

7) High fire resistance.

8) Cosmetic appeal.

Ferro-cement possesses most of the above economic and durable properties. In addition, some of these properties can be altered in the material by the use of additives, especially in the areas of fire resistance, cosmetic appeal and resistance to attack from marine environment.

Plain Portland cement concrete is weak in the above mechanical properties and this represents the primary limitation on its use in marine construction. However, the addition of closely spaced wire reinforcement in the form of mesh or fiber can increase the above mechanical properties to allowable levels for marine construction.

Romualdi (9) (10) has shown how this increases the modulus of rupture of Portland cement concrete. This has been substantiated by other investigators (6) (8) (15) (25). McKenny (27), Collins (26) and Mandel (11) have shown that tensile strength of concrete is increased by closely spaced steel reinforcement. Bailey (21) and Sanday (18) have shown that steel fibrous reinforcement enhances the fatigue characteristics of Portland cement concrete. Romualdi (17) has also shown that steel fibrous reinforcement increases the fracture toughness and resistance to impulsive loading of Portland cement concrete. This has been substantiated by Williamson (14) (19). Investigators have found that mesh reinforcement does not appear to alter the compressive strength of Portland cement concrete (25) but fibrous reinforcement improves it somewhat (14) (19). These results depend on the method of loading but it is obvious that the more random nature of the fibrous reinforcement would provide a greater stiffness in all directions (22) and thus delay compressive failure of the concrete. A recent summary of the engineering properties found by various investigators for mesh and fibrous reinforced ferro-cement is contained in reference (28) by the author.

True two-phase behavior of the material has been found in most experimental work. It would appear from the above research that ferro-cement can be an acceptable material for marine construction. From the practical side, the

present level of boat building activity using the material and the number of successful boats points toward more widespread future use for marine application. The full capability of the material has not been utilized as evidenced by some of the startling results obtained by Collins (26) and Romualdi (17). Balancing this, there is also a relatively wide scattering of data regarding the engineering properties (28). Regardless of these limitations, ferro-cement is being used in marine construction and some form of approximate design technique is required to aid the marine engineer. An especially weak area is the bending of plates since most of the experimental data available deals with the bending of beams or standard experimental tests for determining the material properties. Since a major portion of marine structures consist of plate construction a plate design technique for this material with experimental verification would be particularly useful. This is the purpose of this thesis.

II THEORY

A. Mechanism of Fracture in an Elasto-Plastic Material

Failure of a material under tensile loading normally occurs through propagation of a crack through the material normal to the axis of loading. A mechanism explaining this behavior has been advanced by Griffith (30) using an energy balance concept. Griffith postulated that the change in total energy occuring as the result of a crack passing through a material is:

$$\Delta W = \Delta T - \Delta U \qquad (1)$$

where: ΔW = Change in total energy of material

ΔT = Change in surface energy

ΔU = Change in elastic strain energy

Griffith calculated the decrease in strain energy due to formation of a line crack of length 2C and of unit thickness to be:

$$\Delta U = \frac{\pi c^2 \sigma^2 (1-\nu^2)}{E} \qquad \text{plain strain} \qquad (2a)$$

$$\Delta U = \frac{\pi c^2 \sigma^2}{E} \qquad \text{plane stress} \qquad (2b)$$

He calculated the resulting increase in surface energy per unit thickness as:

$$\Delta T = 4 \gamma c \qquad (3)$$

where γ = specific surface energy required for formation of a unit area of surface.

Griffith's hypothesis was that the crack would begin to propagate unstably if:

$$\frac{d(\Delta W)}{dc} = 0$$

(e.g. when the rate of change of incremental strain and surface energy changes were equal). This results in the criterion:

$$2\gamma = \frac{\pi c \sigma^2}{E} \tag{4}$$

Irwin (4) has indicated that a modification to the Griffith theory should be made to allow for plastic work in a material prior to fracture. This modification would take the form:

$$2(\gamma + W_p) = \frac{\pi c \sigma^2}{E} \quad \text{plane stress} \tag{5a}$$

$$2(\gamma + W_p) = \frac{\pi c \sigma^2 (1-\nu^2)}{E} \quad \text{plane strain} \tag{5b}$$

Irwin has also developed a theory of rupture by considering the stress field in the immediate vicinity of the crack tip. His theory mades use of analytical stress functions to describe the stress field ahead of the crack and a stress intensity factor (K) to indicate the stress at the tip of the crack. The decrease in strain energy of the material due to formation of a unit

crack length is related to the stress intensity factor (K) by:

$$\frac{d(\Delta U)}{dc} = \frac{\pi K^2}{E} \qquad (6)$$

Comparison of this equation to the Griffith criterion shows that:

$$K = \sigma\sqrt{c} \qquad (7)$$

Irwin defines the strain energy release rate as:

$$G = \frac{\pi K^2}{E} \quad \text{or} \quad G = \frac{\pi \sigma^2 c}{E} \qquad (8)$$

When the crack becomes unstable, the strain energy release rate (G) at this point is designated the critical strain energy release rate (G_c). Irwin suggests that this is a property of the material.

B. Mechanism of Fracture In Ferro-Cement

As developed above it can be seen that a material may be made more resistant to fracture by decreasing the strain energy release rate below the critical value:

$$G < G_c$$

This can be accomplished by:

a) Increasing the modulus of elasticity (E).

b) Reducing the applied stress (σ).

c) Reducing the flaw or crack size.

Unfortunately increasing the modulus of elasticity above certain maximum limits is not normally possible in unreinforced Portland cement concrete. Reduction of the applied stress defeats the goal of efficient use of material. Reduction of flaw size is sometimes difficult under present production methods and is bounded by the naturally occuring flaws in concrete which are on the order of the critical flaw size for tensile stress of 200-400 psi. Some success has been obtained by Moavenzadeh (et al) (24) in increasing the tensile strength of cement mortar by addition of strong sand and other aggregate causing cracks to detour thus increasing the crack path. Substantial side cracking occurs along the main crack thus increasing the crack length and adding to the surface energy. This enhances the material toughness and increases of up to 10% in tensile strength can be obtained in this manner.

However, fracture toughness and tensile strength of the material can also be enhanced if some mechanism could be found which would reduce the stress at the flaw tip, thereby reducing the stress intensity factor (K) below that which causes the critical strain energy release rate.

The use of closely spaced discontinuous or continuous wire reinforcement could aid in reducing the stress concentration at the crack tip. Romauldi and others (9) (10) (11) (17) (18) have done much work in this area. The basic

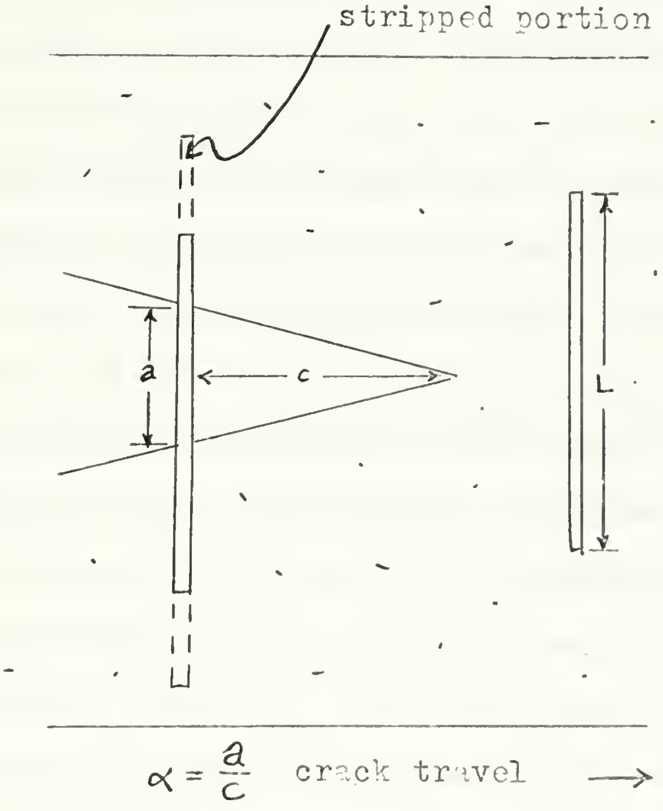

Crack Traversing Fiber Reinforced Matrix

Figure 1

mechanism postulated by Romualdi is that of a line crack traversing through a material (fig. (1)) being stopped by the "pinching" action of the shear bond between the wire reinforcement and the mortar. The stress (strain) ahead of the crack is greater than the average stress (strain) in the material and reinforcement. Thus, assuming a shear bond exists between mortar and wire, the requirement for continuity between mortar and wire at the bond interface will cause the wire to assume much of the stress or essentially cause a "pinching off" of the crack. This action reduces the stress intensity factor (K) or strain energy release rate (G) below the critical value (G_c) required for unstable propagation of the crack.

The effect of wire reinforcement continues even when the crack has passed by the wire. As the shear bond is overcome, irrecoverable work is done either "stripping" of the wire out of the mortar or, if the shear bond is stronger, necking and ductile fracture of the wire. Thus, by this mechanism not only can the strain energy release rate (G) be reduced below the critical value (G_c) due to reduction of stress at the crack tip, but prevention of brittle fracture in the material occurs because of the work of wire "stripping" and/or ductile fracture.

Romualdi has postulated the following formula for the critical strain energy release rate based on the work required to initiate stripping of the wire from the mortar:

(discontinuous wire reinforcement)

$$G_c = \frac{\tau_b \pi d L \alpha}{4 \lambda^2} \qquad (9)$$

where τ_b = shear bond strength

α = ratio of crack width to length at given point

λ = average wire spacing

L - length of wire

d = diameter of wire

He further derived from statistical considerations a formula for the average wire spacing:

$$\lambda = \frac{13.8\ d}{V_f^{.5}} \qquad (10)$$

where V_f = volume percent of reinforcement.

Romauldi's experiments as well as others (28) have shown that the fracture toughness is a very strong function of wire spacing which would tend to bear out his formulation of (G_c). However, much work remains to be done in the area of the bond strength and its affect on (G_c).

C. Bending of Plates

As pointed out previously ferro-cement unlike concrete, possesses the capability for plastic as well as elastic behavior by means of the bond between the reinforcing material and the mortar.

Any design technique would necessarily consider both phases of this behavior. Because of the orthotropic nature

of the material it is also natural to consider numerical techniques for use as an accurate design method. Whang (29) has developed a finite element computer program for the elasto-plastic analysis of orthotropic plates and shells. This program will be used with input of experimentally obtained orthotropic properties, to determine its feasibility as a design method for elasto-plastic plate bending of ferro-cement. The computer output will be compared with experimental results of three basic forms of the material:

Series A: Continuous wire mesh reinforcement, where it is expected that the x and y axes are symmetrical and variation of properties occurs in the direction 45 degrees to these axes. The approach will consider the input of equivalent composite properties.

Series B: Combination of continuous wire mesh and short random fiber reinforcement.

Series C: Short random fiber reinforcement, where it is expected that the material is isotropic in the x y plane but orthotropic in the x z and y z planes. The approach will consider input of composite properties.

1. Orthotropic Constitutive Relations

Ferro-cement is basically orthotropic in nature when

considered in the geometry of plates. With mesh reinforced ferro-cement, the layers of mesh are orthotropic in their plane thereby creating a three dimensional orthotropic material. With fibrous reinforced ferro-cement, the random nature of the fibers causes the material to approach the isotropic condition in the plane of the plate but remain orthotropic normal to the plane of the plate.

Jayne andSuddarth (31) give the constitutive (Hookian) relationships in matrix form for 3-dimensional orthotropic materials. These relations imply that the specific directional properties of the material must be known in order to formulate a design method for such a material. The three dimensional orthotropic constitutive relations are:

$$\begin{vmatrix} \gamma_{11} \\ \gamma_{22} \\ \gamma_{33} \\ \gamma_{23} \\ \gamma_{13} \\ \gamma_{12} \end{vmatrix} = \begin{vmatrix} 1/E_1 & -\nu_{12}/E_2 & -\nu_{13}/E_3 & 0 & 0 & 0 \\ -\nu_{21}/E_1 & 1/E_2 & -\nu_{23}/E_3 & 0 & 0 & 0 \\ -\nu_{31}/E_1 & -\nu_{32}/E_2 & 1/E_3 & 0 & 0 & 0 \\ 0 & 0 & 0 & 1/G_{23} & 0 & 0 \\ 0 & 0 & 0 & 0 & 1/G_{13} & 0 \\ 0 & 0 & 0 & 0 & 0 & 1/G_{12} \end{vmatrix} \begin{vmatrix} \sigma_{11} \\ \sigma_{22} \\ \sigma_{33} \\ \sigma_{23} \\ \sigma_{13} \\ \sigma_{12} \end{vmatrix} \qquad (11)$$

It should be noted that these constitutive relations apply to a specific material. In this work a combination of two materials, steel and cement mortar, is under consideration. The hypothesis is that the combination of these materials results in a new material which has properties that follow the theory of fiberous composites (34). As such the material can be treated using the above constitutive relations in arriving at a plate bending theory and composite properties may be used as input to this theory.

2. Elastic Plate Bending

The basic differential equilibrium equation for pure bending of plates is:

$$\frac{\partial^4 w}{\partial x^4} + 2\frac{\partial^4 w}{\partial x^2 \partial y^2} + \frac{\partial^4 w}{\partial y^4} = \frac{q}{D} \qquad (12)$$

where: w = displacement normal to plane of plate

q = loading/unit area

D = flexural rigidity of plate

Timoshenko (32) has developed the theory for elastic bending of plates and shells of homogeneous isotropic material where: (13)

$$D = \frac{E h^3}{12(1-\nu^2)}$$

For the general case of bending of simply supported rectangular plates under a uniform load (q_0), Timoshenko

obtained the solution:

$$w = \frac{16 q_o}{\pi^6 D} \sum_{m=1}^{\infty} \sum_{n=1}^{\infty} \frac{\sin \frac{m\pi x}{a} \quad \sin \frac{n\pi y}{b}}{mn \left(\frac{m^2}{a^2} + \frac{n^2}{b^2} \right)^2} \qquad (14)$$

where: m - odd

n - odd

a and b are dimensions of plate sides

This has been specialized for partial loading for the case of a concentrated load (P) at the center of a square plate (fig. 2) as:

$$w\Big|_{y=0} = \frac{P a^2}{2 D \pi^3} \sum_{m=1}^{\infty} \frac{\sin \frac{m\pi}{2}}{m^3} \left(\tanh \frac{m\pi}{2} - \frac{m\,\pi/2}{\cosh^2 m\pi/2} \right) \sin \frac{m\pi x}{a} \qquad (15)$$

and the maximum deflection reduces to:

$$w\Big|_{\substack{y=0 \\ x=c}} = \frac{\alpha P a^2}{E h^3} \qquad (16)$$

where: α = solution to the infinite series for x = a/2

The displacement along the y axis is found by interchanging x with y in the above expression.

The bending moments along the x and y axis can be found from the curvatures using the basic relations:

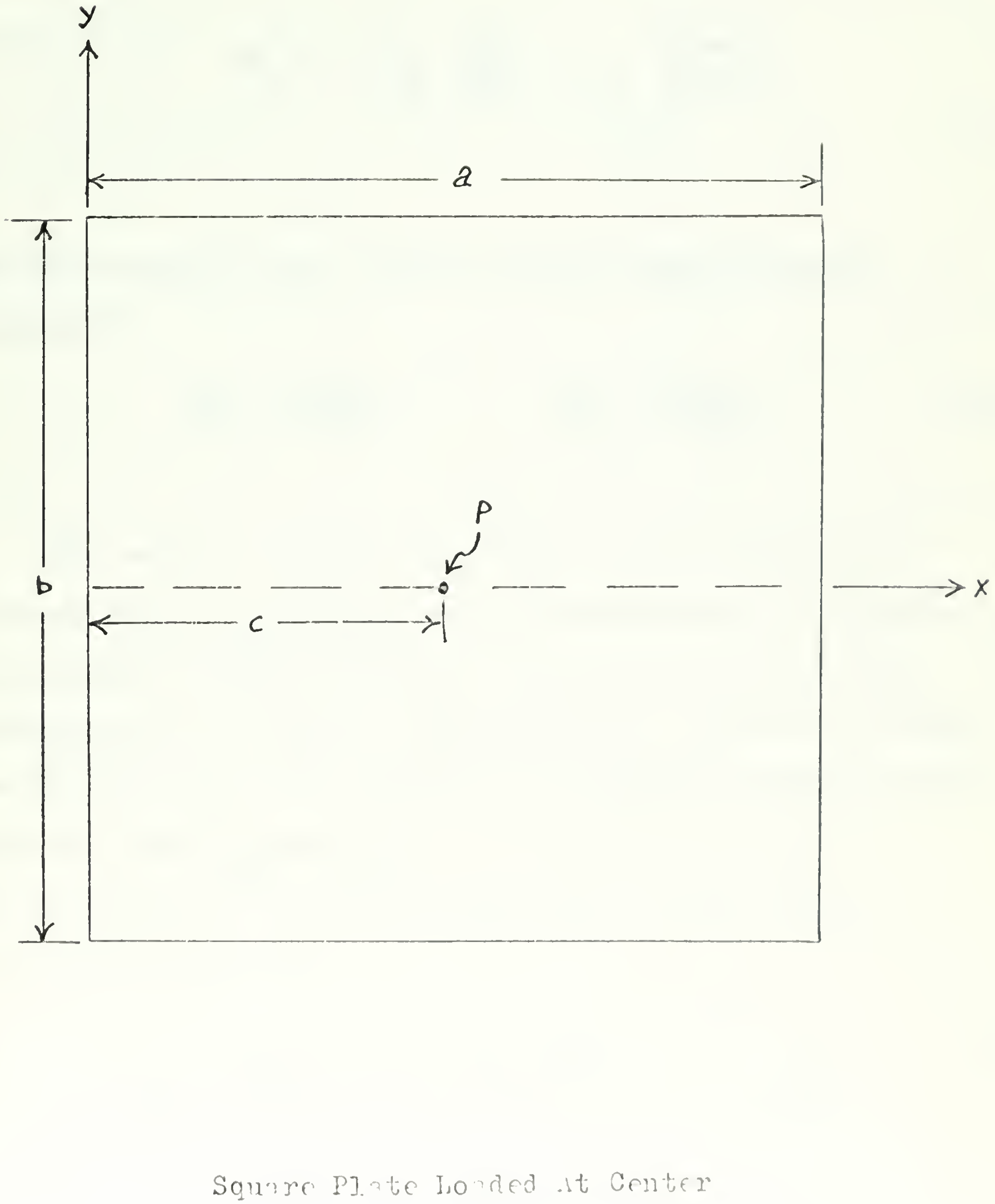

Square Plate Loaded At Center

Figure 2

$$M_x = -D\left(\frac{\partial^2 w}{\partial x^2} - \nu \frac{\partial^2 w}{\partial y^2}\right) \qquad (17)$$

$$M_y = -D\left(\frac{\partial^2 w}{\partial y^2} - \nu \frac{\partial^2 w}{\partial x^2}\right)$$

and the stresses can be found from the basic flexural relations:

$$\sigma_x = \frac{6M_x}{h^2} \qquad \sigma_y = \frac{6M_y}{h^2} \qquad (18)$$

The bending moments and stress in the vicinity of a concentrated load (fig.2) are not satisfactory if calculated using the above equation. They must be found using superposition of moments from bending of a centrally loaded rectangular plate and bending of a centrally loaded circular plate of radius $\frac{2a}{\pi}\sin\frac{\pi c}{a}$.

The solution for the moment along the x axis of the rectangular plate is:

$$M_x = \frac{P(1+\nu)}{4\pi}\operatorname{Log}\frac{2a\sin\pi c/a}{\pi r} + \gamma_1\frac{P}{4\pi} \qquad (19)$$

where: $r = \sqrt{y^2 + (x-c)^2}$

γ_1 = numerical factor depending on ratio of sides of plate.

The solution for the moments near the center of a centrally loaded circular plate is:

$$M_x = \frac{P}{4\pi}(1+\nu) \operatorname{Log} \frac{a}{r} + (1-\nu) \frac{P y^2}{4\pi r^2} \tag{20}$$

Assuming the circular plate is of radius $\frac{2a}{\pi} \sin \pi c/a$, then near the center of the plate the two solutions are identical except for the uniform bending term $\gamma_1 \frac{P}{4\pi}$. The solution for the moment at the center of a circle of radius (a) where P is now uniformly distributed over an area of radius (e) is:

$$M = \frac{P}{4\pi}\left((1+\nu) \operatorname{Log} \frac{a}{e} + 1\right) \tag{21}$$

Superposing the constant additional moment of $\gamma_1 \frac{P}{4\pi}$ from the rectangular plate the expression for the moment at the center of the rectangular plate becomes:

$$M_x = \frac{P}{4\pi}\left((1+\nu) \operatorname{Log} \frac{2a \sin \pi c/a}{\pi e} + 1\right) + \frac{\gamma_1 P}{4\pi} \tag{22}$$

The stresses may be found as before from the basic flexural relations.

Now for anisotropic materials in plane stress such as bending of ferro-cement plates the basic differential equilibrium equation becomes:

$$D_x \frac{\partial^4 w}{\partial x^4} + 2(D_1 + 2D_{xy}) \frac{\partial^4 w}{\partial x^2 \partial y^2} + D_y \frac{\partial^4 w}{\partial y^4} = q \qquad (23)$$

where:

$$D_x = \frac{E_x \quad h^3}{(1-\nu^2)\ 12}$$

$$D_y = \frac{E_y \quad h^3}{(1-\nu^2)\ 12}$$

$$D_1 = \frac{\nu E_y\ h^3}{(1-\nu^2)\ 12} \quad ; \qquad \frac{\nu E_x\ h^3}{(1-\nu^2)\ 12}$$

$$D_{xy} = \frac{G\ h^3}{12}$$

Exact solutions have been obtained by Timoshenko for the case of a uniformly loaded plate and by Huber (33) for concentrated loads in the elastic range. However, since the purpose of this paper is to investigate also the plastic behavior of the material, numerical methods are better suited to carry out the analysis.

The inclusion of membrane stress in the elastic bending of plates is described by the following nonlinear differential equations:

$$\frac{\partial^4 F}{\partial x^4} + 2 \frac{\partial^4 F}{\partial x^2 \partial y^2} + \frac{\partial^4 F}{\partial y^4} = E\left[\left(\frac{\partial^2 w}{\partial x \partial y} \right)^2 - \frac{\partial^2 w}{\partial x^2} \frac{\partial^2 w}{\partial y^2} \right] \qquad (24\ a)$$

$$\frac{\partial^4 w}{\partial x^4} + 2\frac{\partial^4 w}{\partial x^2 \partial y^2} + \frac{\partial^4 w}{\partial y^4} = \frac{h}{D}\left(\frac{q}{h} + \frac{\partial^2 F}{\partial y^2}\frac{\partial^2 w}{\partial x^2} + \frac{\partial^2 F}{\partial x^2}\frac{\partial^2 w}{\partial y^2} - 2\frac{\partial^2 F}{\partial x \partial y}\frac{\partial^2 w}{\partial x \partial y}\right) \quad (24b)$$

where F is a stress function satisfying the elemental equilibrium equations for normal forces (N) and is defined as:

$$N_x = \frac{\partial^2 F \; h}{\partial y^2} \; ; \; N_y = \frac{\partial^2 F \; h}{\partial x^2} \; ; \; N_{xy} = -\frac{\partial^2 F \; h}{\partial x \partial y} \qquad (25)$$

The general solution to the above equation is not known, therefore numerical techniques must be utilized to find w, F and subsequently the normal forces, moments and stresses.

3. Plastic Plate Bending

Prandtl-Reuss Plastic Flow Rule

Figure 3 shows the stress strain curve for an elasto plastic material. At the onset of plastic yielding the relation between plastic strains and stresses can be described by the following plastic flow rule:

Perfectly plastic material

$$d\epsilon^p = d\lambda \, \nabla f \qquad (26)$$

$d\lambda$ = Positive constant

$d\epsilon^p$ - Incremental Plastic strain

∇f - Gradient of yield function

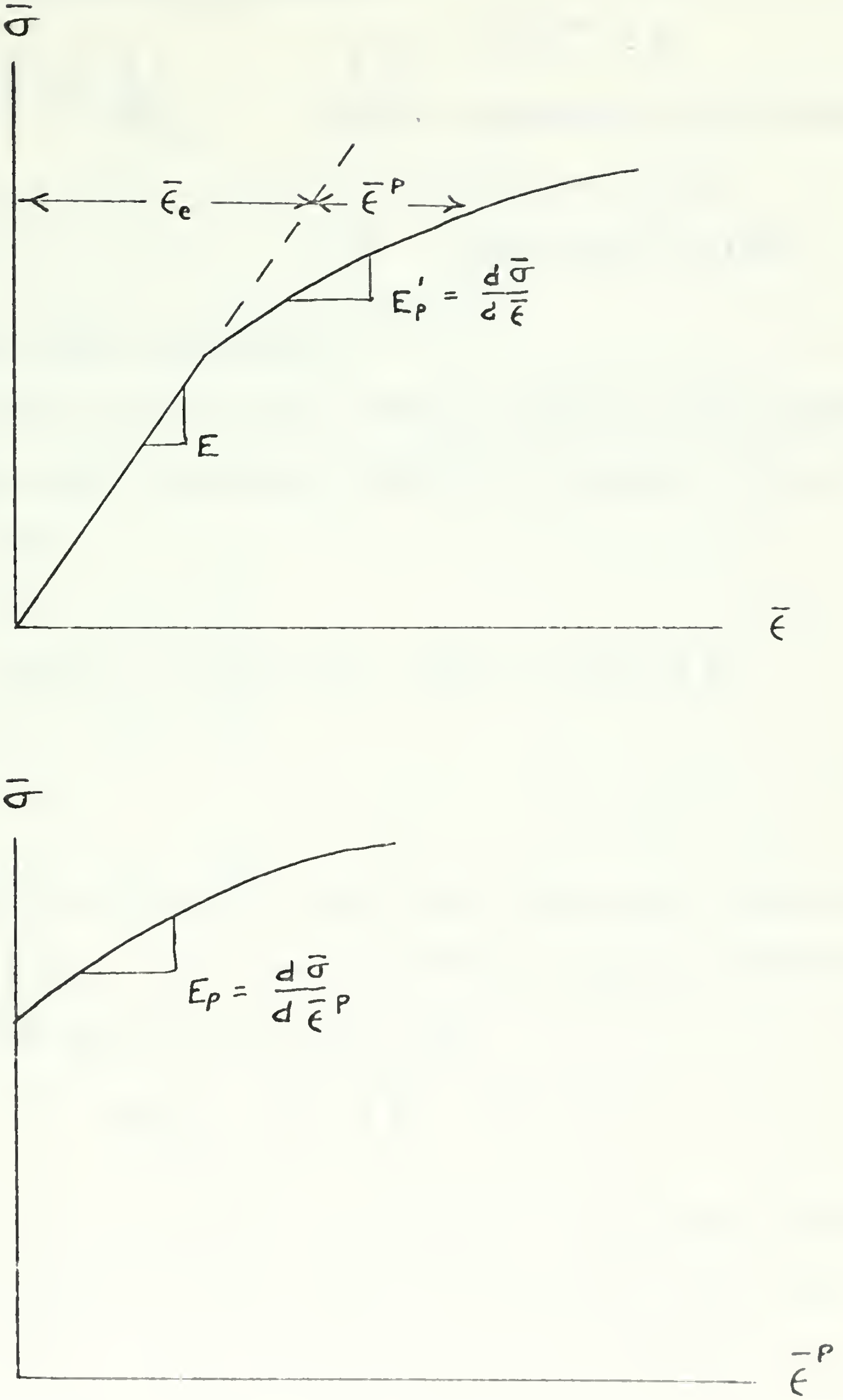

Stress-Strain Curve For Elasto Plastic Material

Figure 3

Strain hardening material

$$d\epsilon_{ij}^{p} = d\lambda \frac{\partial f}{\partial \sigma_{ij}}$$

$d\lambda = h(d\bar{\epsilon}^{p}, \bar{\sigma})$

$d\bar{\epsilon}^{p}$ = Incremental equivalent plastic strain (27)

$\bar{\sigma}$ = Equivalent stress

Huber-Mises Yield Criterion

Using the distortional energy concept of the popular Huber-Mises yield criterion the yield function (f) can be expressed as:

$$2f = 2\bar{\sigma}^{2} = (\sigma_1 - \sigma_2)^2 + (\sigma_2 - \sigma_3)^2 + (\sigma_3 - \sigma_1)^2 \qquad (28)$$

The relation between the equivalent stress and incremental plastic strain is the area beneath the plastic stress strain curve or the plastic work Wp. Thus:

$$dW_p = \bar{\sigma}\, d\bar{\epsilon}^{p} \qquad (29)$$

Incremental Stress Strain Relations for Isotropic Material

Substitution of the yield function (f) into the strain hardening flow rule results in the plastic incremental stress strain relations for a strain hardening material such as steel. If we also note that:

$$dW_p = 2\bar{\sigma}^2 d\lambda \quad ; \quad d\lambda = \frac{d\bar{\epsilon}^{p}}{2\bar{\sigma}} \qquad (30)$$

Then the form of the incremental plastic stress strain relations become:

$$
\begin{aligned}
d\epsilon_x^p &= \left[\sigma_x - \tfrac{1}{2}(\sigma_y + \sigma_z)\right] \frac{d\bar{\epsilon}^p}{\bar{\sigma}} \\
d\epsilon_y^p &= \left[\sigma_y - \tfrac{1}{2}(\sigma_x + \sigma_z)\right] \frac{d\bar{\epsilon}^p}{\bar{\sigma}} \\
d\epsilon_z^p &= \left[\sigma_z - \tfrac{1}{2}(\sigma_x + \sigma_y)\right] \frac{d\bar{\epsilon}^p}{\bar{\sigma}} \\
d\epsilon_{xy}^p &= \frac{3}{2}\,\tau_{xy} \frac{d\bar{\epsilon}^p}{\bar{\sigma}} \\
d\epsilon_{yz}^p &= \frac{3}{2}\,\tau_{yz} \frac{d\bar{\epsilon}^p}{\bar{\sigma}} \\
d\epsilon_{zx}^p &= \frac{3}{2}\,\tau_{zx} \frac{d\bar{\epsilon}^p}{\bar{\sigma}}
\end{aligned}
\qquad (31)
$$

Incremental Stress Strain Relations for Orthotropic Material

By introducing parameters of anisotropy (Aij) as coefficients of the various terms of the yield criterion, the anisotropic plastic stress strain relations may be obtained through use of the flow rule as before. Thus:

$$
d\epsilon_{11}^p = \frac{1}{2}\left(A_{11}\,\sigma_{11} - A_{12}\,\sigma_{22} - A_{31}\,\sigma_{33}\right) \frac{d\bar{\epsilon}^p}{\bar{\sigma}} \qquad (32)
$$

$$d\epsilon_{22}^{p} = \frac{1}{2}\left(-A_{12}\,\sigma_{11} + A_{22}\,\sigma_{22} - A_{32}\,\sigma_{33}\right)\frac{d\bar{\epsilon}^{p}}{\bar{\sigma}}$$

$$d\epsilon_{33}^{p} = \frac{1}{2}\left(-A_{31}\,\sigma_{11} - A_{32}\,\sigma_{22} + A_{33}\,\sigma_{33}\right)\frac{d\bar{\epsilon}^{p}}{\bar{\sigma}}$$

$$d\epsilon_{12}^{p} = \frac{3}{2}\,A_{44}\,\tau_{12}\,\frac{d\bar{\epsilon}^{p}}{\bar{\sigma}}$$

$$d\epsilon_{23}^{p} = \frac{3}{2}\,A_{55}\,\tau_{23}\,\frac{d\bar{\epsilon}^{p}}{\bar{\sigma}}$$

$$d\epsilon_{31}^{p} = \frac{3}{2}\,A_{66}\,\tau_{31}\,\frac{d\bar{\epsilon}^{p}}{\bar{\sigma}}$$

The Aij are material dependant and may be obtained from tensile tests and shear tests.

If the analysis is reduced to plane stress condition which is usually assumed in plate bending then the only non zero Aij are A11, A12, A22, A44 since $\tau_{zy} = \tau_{zx} = \sigma_z = 0$ is then assumed. These Aij can then be obtained through 3 tensile and one shear test.

The initial values of these parameters are:

$$\begin{aligned} A_{11} &= 2\left(\frac{\bar{\sigma}_{\text{yield}}}{\sigma_{x\ \text{yield}}}\right)^2 \\ A_{22} &= 2\left(\frac{\bar{\sigma}_{\text{yield}}}{\sigma_{y\ \text{yield}}}\right)^2 \\ A_{44} &= \frac{1}{3}\left(\frac{\bar{\sigma}_{\text{yield}}}{\tau_{xy\ \text{yield}}}\right)^2 \end{aligned} \qquad (33)$$

$$A_{12} = 1 + 2A_{22} + 3A_{44} - \left(\frac{2\,\bar{\sigma}_{\text{YIELD}}}{\sigma_{45^\circ\,\text{YIELD}}}\right)^2$$

For a strain hardening material these parameters will change as $\bar{\sigma}$, σ yield, τ yield vary.

As has been previously indicated in order to solve the plastic behavior of plate bending numerical methods are required. There are two basic methods for incremental elasto-plastic analysis. In the case of simple tension they are described as:

(1) Initial stiffness where the predicted strain $\Delta U/L$ for given $\Delta P/A$ is found by using the elastic modulus E but varying the initial load $\Delta P_0/A$ to approach final agreement with the stress strain curve (point B Fig. 4)

$$\frac{\Delta P}{A} + \frac{\Delta P_o}{A} = E\,\frac{\Delta U}{L} \tag{34}$$

(2) Tangent stiffness where the tangent modulus E_t is found and improved upon at each iteration to yield the strain $\Delta U/L$ that will agree with the stress strain curve for a given loading $\Delta P/A$.

$$\frac{\Delta P}{A} = E_t\,\frac{\Delta U}{L} \tag{35}$$

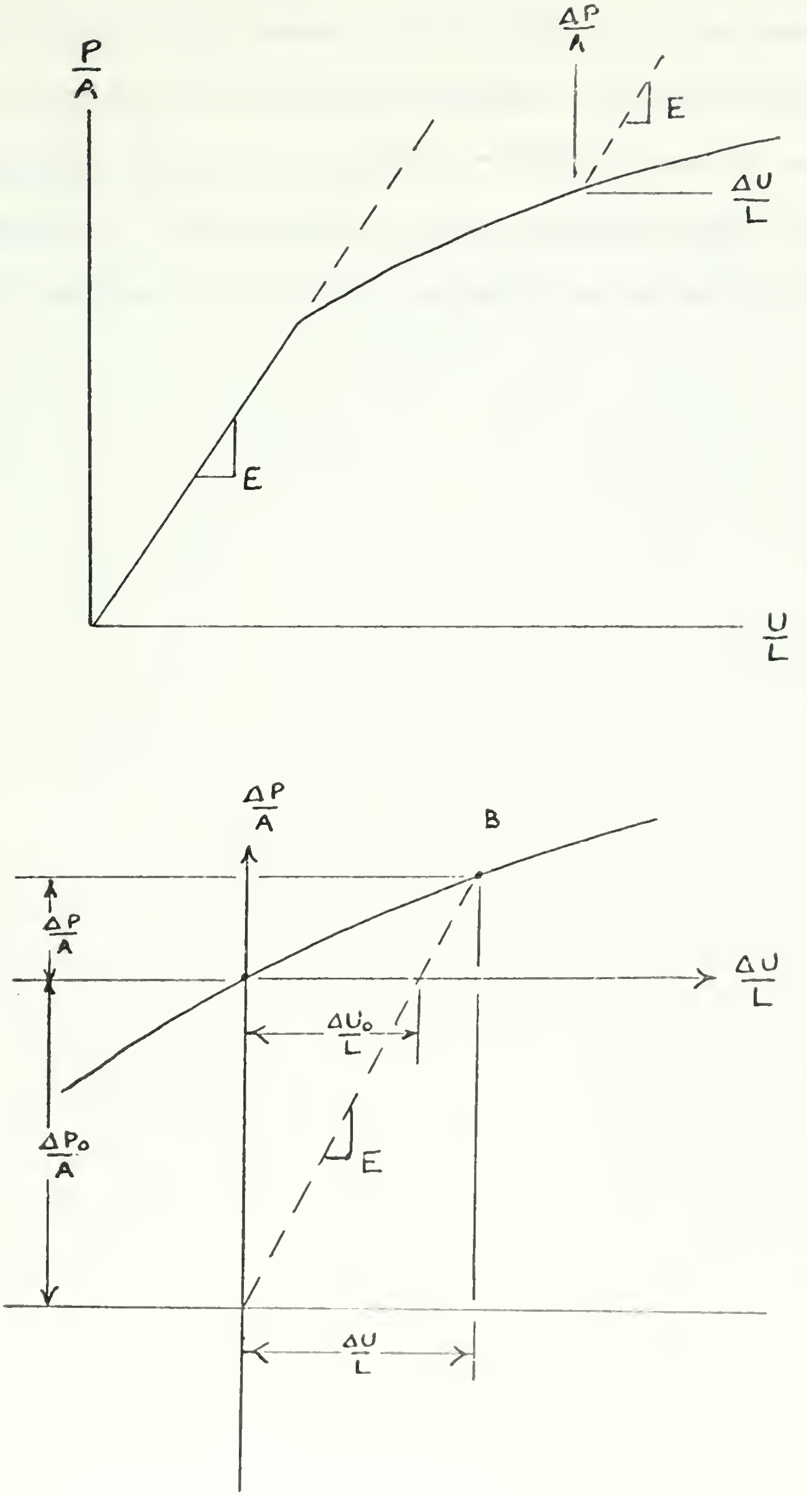

Incremental Elasto-Plastic Analysis Method: Simple Tension

Figure 4

Whang (29) has used these two methods in constructing a finite element iterative technique which solves for the stresses, strains, moments and displacement of the plate surface. The output of the program using the initial stiffness approach, will be compared to experimental results.

III EXPERIMENTAL PROCEDURE

A. Plate Bending

Three sets of ferro-cement plate specimens were tested incorporating continuous wire mesh reinforcement (series A), discontinuous short random fiber reinforcement (series C), and a combination of these in equal proportions (series B). Table I shows the specifications for each set of plates. All plates were square, 10" on an edge and .5 ± .03" thick. The method of lay up was the same for all plates. The fibers were added to the mortar as it was being wet mixed in the mixer. The mesh reinforcement was laid into the form after a thin layer of mortar had been placed. Then mortar was placed upon the mesh. All specimens were vibrated in the molds 15-30 seconds. Eight specimens were made with each batch of mortar. A total of sixteen specimens of each plate type were made. The forms for initial lay up consisted of a formica backboard and 1/2" wooden boundry strips. The forms were oiled prior to each use. All plate specimens were cured under water.

The testing program was designed to compare the load deflection curve of the center point of the various plate types when loaded with a concentrated load at the center. Each plate was simply supported on the edges by a rigid pipe frame and loaded at the center as shown in Figure 5.

Plate Series	Steel Reinforcement Type	% Wt.	Cement Type	Aggregate	W/C	C/S
A	4 layers 4/in. M.S .042 in. dia. woven wire mesh (bright)**	20.85	I	Ottawa C-109 fine sand	.466	.66
B	2 layers 4/in. M.S .042 in. dia. woven wire mesh	10.42	"	"	"	"
	3/4" X .016" round H.T.S. wire fibers (bright)*	10.43				
C	3/4" X .016" round H.T.S. wire fiber (bright)	20.85	"	"	"	"
Cylinder Series						
I	Unreinforced	0.0	"	"	"	"
II	3/4" X .016 round H.T.S. wire fibers (bright)	20.85	"	"	"	"
III	"	10.43	"	"	"	"

All plate specimens were cured for 109 days and all cylinder specimens were cured for 68 days.

** Wire mesh UTS = 42,300 psi

* Wire fiber UTS = 140,000 psi

MATERIAL SPECIFICATIONS

TABLE I

The plates were loaded until ultimate failure of the wire or wire/mortar bond occured. The deflection of other points on the plate surface was measured at the point of ultimate bending failure in order to obtain the relative curvature of the plate surface. The center point load deflection curve is compared with the results of the finite element numerical analysis in the following section.

B. Material Properties

For prediction of the plate bending behavior it is necessary to obtain certain properties of the material to use as input to the computer analysis. For this purpose three of the plates in each series were cut with a diamond tipped saw into 1" wide strips. These strips were tested in flexure, tension and shear on the Instron universal testing machine at a deflection rate of .05"/min. The following properties of each series were obtained in the x, y, and 45° directions:

Tensile yield stress σ_y
Flexural yield stress σ_y
Youngs modulus E
Plastic Modulus E_p
Shear yield stress τ_y

Poissons ratio (ν) was assumed to be that of cement mortar reported in the literature ($\nu = 0.2$). The shear modulus (G) was assumed to obey the relation:

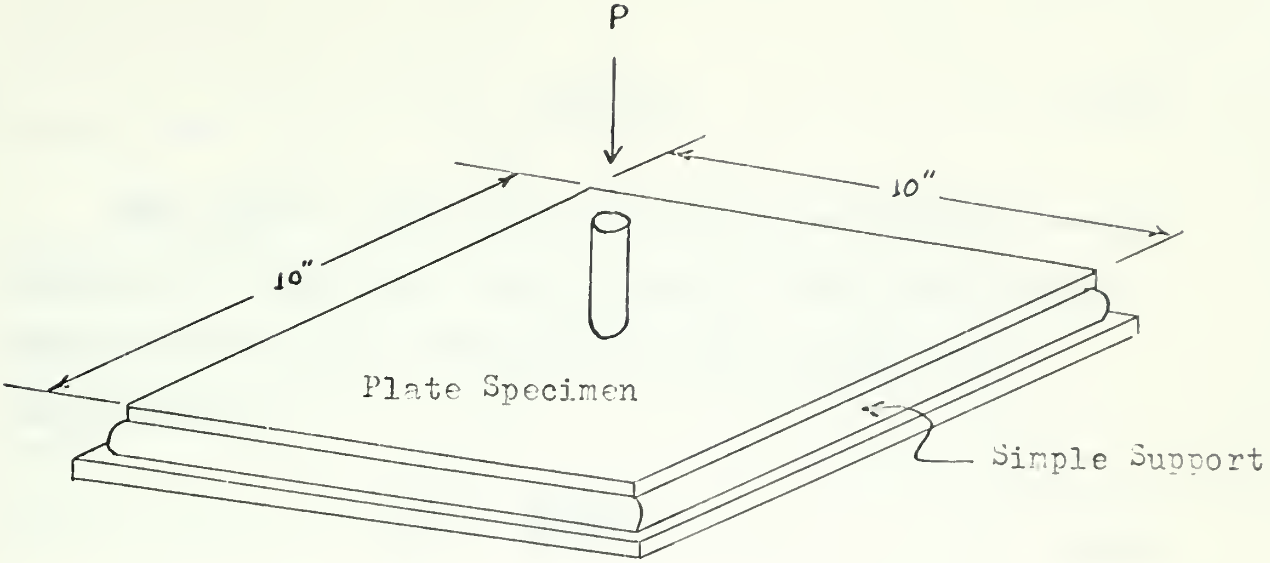

Method of Plate Loading

Figure 5

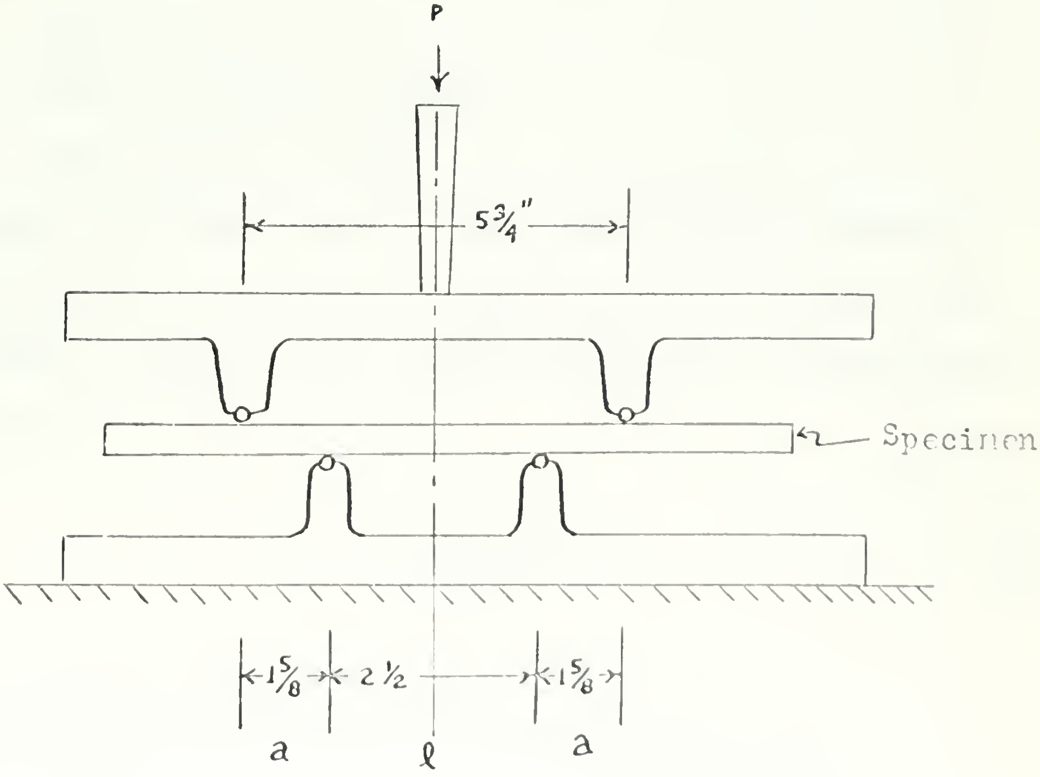

Flexure Test Apparatus

Figure 6

$$G = \frac{E}{2(1+\nu)} \tag{36}$$

The flexure test was conducted on the Instron testing machine and employed 4 point bending of the specimens as shown in figure 6. The flexural yield stress was calculated by:

$$\sigma_y = \frac{a P_y h}{4 I} \tag{37}$$

where: a = distance between outer and inner supports.

$I = \frac{1}{12} b h^3$

P_y = load at yield

h = specimen thickness

b = specimen width

The yield point was taken as the first marked deviation from linearity on the load deflection curve. (figure 24) The Young's modulus was calculated from the end deflction formula for 4 point bending:

$$E = \frac{P a^2 (2a + 3l)}{6 I \delta} \tag{38}$$

where: l = distance between inner supports

δ = deflection at end (outer) load point

The plastic modulus was calculated using the same formula but inserting the change in deflection for corresponding

change in load after yield up to ultimate stress. This assumes constant moment of inertia (I) in the plastic region which causes this to be an approximation at best.

The tensile tests were also conducted using the Instron testing machine (fig.7). The test specimens were prepared for the testing machine grips by expoxy bonding (Hysol-IC) 2" lengths of thin steel shim stock (1/64" thickness) to the sample in the area of the grip contact. Tensile yield stress was calculated by:

$$\sigma_y = \frac{P_y}{b\,h} \qquad (39)$$

where the yield point is again taken as the first marked deviation from linearity on the load strain curve. The Young's modulus was obtained by using the strain output from an extensiometer attached to the specimen (figure 7):

$$E = \frac{\sigma_y}{\epsilon_y} \qquad (40)$$

where: ϵ_y = extensiometer strain

The plastic modulus was obtained by using incremental values of stress and strain above the yield point along the line connecting the yield stress and ultimate stress.

The shear tests were also conducted using the Instron testing machine. The shear sample was loaded as shown in figure 8. This form of loading causes some compressive

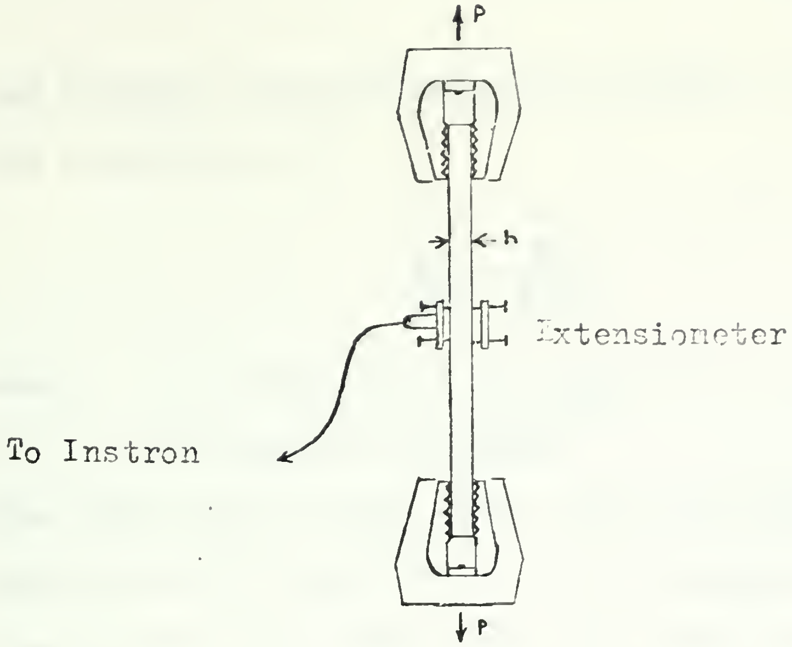

Tensile Test Apparatus

Figure 7

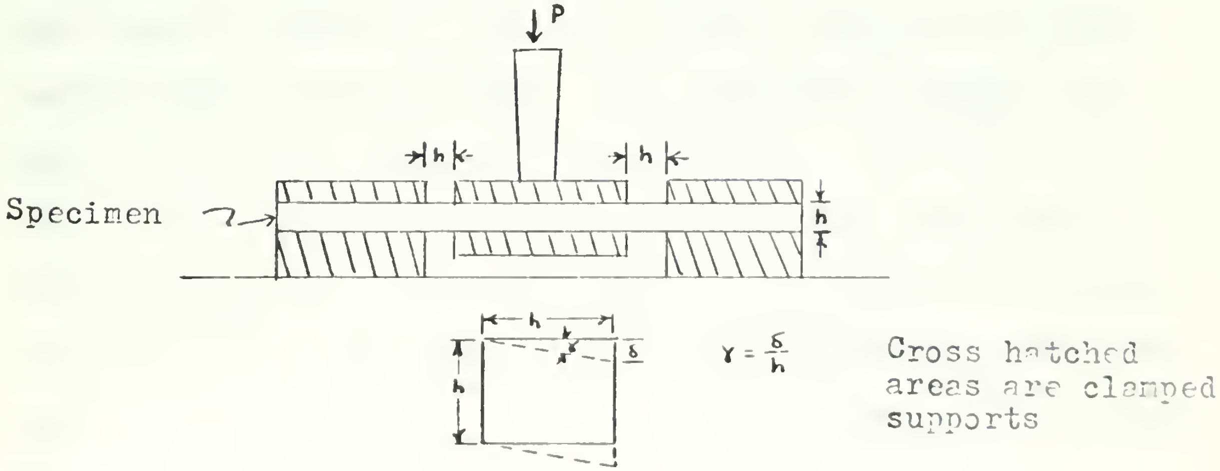
P
h
h
Specimen
h
h
h
δ
$\gamma = \frac{\delta}{h}$
Cross hatched areas are clamped supports

Shear Test Apparatus

Figure 8

[illegible]

[illegible]

and bending forces to enter the results. Shear yield stress was calculated as:

$$\tau_y = \frac{P_y}{2bh} \tag{41}$$

where: b = thickness of specimen

h = height of specimen

The yield point in the above tests was easy to determine because in all cases there was an abrupt change in the slope of the load deflection curve when the first slip of reinforcement and microcracking of matrix occured.

Compressive tests were performed on unreinforced and reinforced cement mortar cylinders to determine the variation of compressive yield strength and the compressive Young's modulus for various volume fractions of short random fiber reinforcement. The compressive modulus for mesh reinforced mortar was not obtained. The effect of the mesh on mortar compressive strength has been found to be negligible (25) when loaded in the plane of the mesh reinforcement. The Young's modulus in compression and tension were compared for the short random fiber reinforcement. The test was conducted according to ASTM C-469-65 for determination of Young's modulus of concrete, except that smaller size cylinders (2" x 4") were used. The yield point in these tests was taken at .002 offset strain and the Young's modulus was calculated on the basis of the

secant slope to this yield point.

IV EXPERIMENTAL RESULTS

Table II summarizes the significant experimental results contained in Appendix I. Figures 9 through 21 show graphically the trends in material properties and plate bending data for the various material types. Again it is emphasized that these properties are equivalent properties which apply to the behavior of the composite material. In general, the results indicate that inclusion of short random fiber reinforcement in cement mortar:

a) Increases the modulus of elasticity.
b) Increases the ultimate compressive stress.
c) Increases the plastic work under the stress strain curve.

The inclusion of short random fibers with corresponding reduction in continuous fiber content in mortar reinforced with continuous fibers causes:

a) An increase of the modulus of elasticity.
b) A decrease in ultimate tensile stress.
c) A decrease in tensile yield stress.
d) An increase in impact energy/area.
e) An increase in the above properties on an axis 45° to x or y axis.
f) Little variation of the plastic modulus.
g) Little variation of shear yield stress.

Plate bending results indicate that inclusion of the

TABLE II

SUMMARY OF EXPERIMENTAL RESULTS

A. Material Properties

Direct Tension Test

	x, y Direction			45° to x, y Direction		
Series	A	B	C	A	B	C
(psi) σ_y	830	608	530	598	594	530
(psi x 10^6) E	2.91	3.5	3.77	3.68	3.55	3.77
(psi) σ_u	1460	1011	721	1003	701	721
(psi x 10^6) E_p	.52	.501	.449	.276	.47	.449

Flexure Tests

	x, y Direction			45° to x, y Direction		
Series	A	B	C	A	B	C
(psi) σ_y	2690	1460	1560	1070	1355	1560
(psi x 10^6) E	1.39	1.22	1.43	1.73	1.19	1.43
(psi) σ_u	4840	3090	2510	2780	2460	2510
(psi x 10^6) E_0	.104	.198	.594	.448	.362	.594

	Shear Test	Impact Test	Unreinforced Mortar Cube Compression Test
Series	τ_y (psi)	ft-lb/in^2	σ_c (psi)
A	1093	90.5	8623
B	1040	109.5	8000
C	805	193.0	7920

Cylinder Compressive Tests

Series	%Random Fiber Content	σ_c (psi)	E (secant .002 offset) (psi x 10^6)
I	0.0	7060	3.2
II	4.75	8775	3.83
III	2.375	8060	3.35

B. Plate Bending Data

Series	Ultimate Bending Load (lb)	Ultimate Membrane Load (lb)	Equivalent Thickness	(ETR)
A	583	1725	.428	1.0
B	816	1150	.472	1.33
C	780	-	.455	1.198

(ETR= Equivalent thickness ratio based on series A)

Normalized Plate Surface Deflection At Ultimate Bending Load

	Station Along x Axis					
Series	Center	2	3	4	5	Edge
A	.0805	.0604	.0473	.0277	.0109	0
B	.146	.0998	.0732	.0535	.0225	0
C	.1258	.0887	.0672	.0449	.0259	0

Normalized Center Point Load-Deflection Curve

Series A		B		C	
Load	Deflection	Load	Deflection	Load	Deflection
100	.0066	100	.0694	100	.00727
150	.00968	150	.01085	150	.01158
200	.0135	200	.015	200	.01578
300	.02505	300	.0207	300	.0251
400	.0404	400	.0334	400	.0395
583	.0805	500	.0428	600	.0678

Normalized Center Point Load-Deflection Curve (continued)

Series A		B		C	
Load	Deflection	Load	Deflection	Load	Deflection
800	.29	600	.0674	780	.1258
1000	.417	816	.146		
1725	.874	1000	.732		
		1150	.98		

short random fibers in lieu of continuous wire reinforcement causes:

a) An increase in ultimate plate bending load.

b) A decrease in ultimate plate membrane load after ultimate bending stress.

c) An increase in plastic work done in deforming the plate.

V DISCUSSION OF RESULTS

A. Material Properties in x, y Directions

1. Tensile Strength

It is expected from the theory of fiberous composites (34) that the strength of the specimens will be highly dependent upon the shear bond between fiber and matrix since the cement mortar matrix in this material does not deform plastically to any appreciable extent. The theories which have been developed for both continuous and discontinuous fiber reinforced composites where the matrix is capable of plastic flow, do not apply in the case of ferro-cement. However Kelly and Davies (34) have advanced a theory for determining the critical transfer length of a *discontinuous* fiber in a purely elastic matrix, based on the coefficient of friction between fiber and matrix:

$$\frac{l_c}{d} = \frac{\sigma_f}{2\mu\sigma_u}\left(\frac{\lambda}{d}\right) \tag{42}$$

where: σ_f = UTS of fiber

σ_u = UTS of matrix

λ = Spacing between fibers

d = Diameter of fiber

l = Length of fiber

μ = Coefficient of friction between fiber and matrix

At fiber lengths below lc the strength of the composite is dependent upon the shear bond of the fiber matrix interface and can be given as:

$$\sigma_c = \sigma_u (1 - V_f) + 2 \eta \sigma_u \frac{\ell}{r} V_f \tag{43}$$

where: V_f = Volume fraction of fibers

When $\ell \geq \ell_c$ the strength of the composite is dependent upon the shear strength of the matrix. This can be given as:

$$\sigma_c = \tau (1 - V_f) + \sigma_f \frac{V_f}{2} \tag{44}$$

where: τ = Ultimate shear strength of matrix

In the case of continuous fiber oriented in the direction of loading in a nonstrain-hardening elastic matrix the strength of the composite is given by:

$$\sigma_c = \sigma_f V_f + \sigma_m' (1 - V_f) \tag{45}$$

where the second term may or may not exist depending on whether the matrix is capable of carrying some stress (σ_m') at the strain where the fibers reach their UTS (σ_f). In most cases with continuous fiber reinforced ferro-cement the second term is zero when the fibers reach σ_f . Using this interpretation of the above equation

the ultimate tensile strength of the mesh reinforced specimens (series A) should be on the order of:

$$\sigma_c = 42{,}300(.0475) = 2010 \text{ psi} \tag{45}$$

The experimental value is 1460 psi. This is lower than the predicted value because not all of the volume of steel is acting in the direction of loading as assumd in the theoretical predition. The theoretical value of ultimate stress considering only the fibers oriented in the direction of load (2.37%) is 1005 psi. This value is below that determined experimentally and indicates that the non oriented fibers contribute partially to resisting load.

Theoretically the strength of the discontinuous fiber specimens (series C) must be less than that of continuous fiber reinforced specimens (series A) (34). In the case of the specimens tested in this thesis the length diameter ratio of the short random fibers is less than the critical value (as shown below) and thus the strength depends upon the shear bond strength. Assuming a nominal UTS of mortar to be 550 psi based on compression strength (36) then:

$$\frac{l_c}{d} = \frac{140{,}000}{2(1.02)550}\left(\frac{.101}{.016}\right) = 790 \tag{42}$$

where the value of y has been taken from (35) and where:

$$\lambda = \frac{13.8\,d}{(V_f)^{.5}} = .101 \qquad (10)$$

This high ℓ_c/d would cause random fibers to be very difficult to work with and it would probably be more advantageous to use continuous mesh fibers. Clearly the ℓ/d for fiber reinforced mortar in this paper is much less than the critical ℓ_c/d :

$$\frac{\ell}{d} = 47 < 790$$

However, based on this ℓ/d the strength of the composite, if all fibers were oriented in the same direction, would be on the order:

$$\sigma_c = 550(.9525) + 2(1.02)550\frac{(.75)}{.101}.0475 \qquad (43)$$

$$= 920 \text{ psi}$$

The experimental value is 721 psi. The actual strength of the mortar could vary from that assumed and thus change this value. It is apparent that random orientation of the fibers has reduced the strength below that predicted for oriented fibers. Nielson and Chen (22) have developed theoretical relations for the variation of properties in fiber reinforced composites using parallel and randomly oriented fibers. For the case discussed here these relations (based on the volume fraction of fibers (4.75) and the

ratio of the elastic modulus of the fiber and matrix material (10)) predict that:

$$\sigma_{c\,\mathrm{random}} = .795\ \sigma_{c\ \mathrm{parallel}} = 732\ \mathrm{psi}$$

which is quite close to the experimental value.

The modulus of rupture in flexure follows the above trend. Plots of tensile and flexure results are shown in figures 9 through 12. Examination of these results reveals that in all cases UTS is affected to a greater extent by the difference in reinforcement type while the yield stress decreases at a lesser rate with the shift to discontinuous fiber reinforcement.

2. Modulus of Elasticity

The modulus of elasticity increases with discontinuous fiber reinforcement. This is borne out in the cylinder compression tests and tension tests. The result is more apparent in the direct tension test than in the flexure tension tests. Since the modulus is measured directly in the direct tension test this value is to be preferred over that of the flexure specimens. The reduced flexure data is very dependent on the location of the neutral axis which was approximated in the test results as h/2. This could vary significantly depending on the location of any concentration of reinforcement. For this reason direct tension test results are used exclusively as input to the finite element analysis.

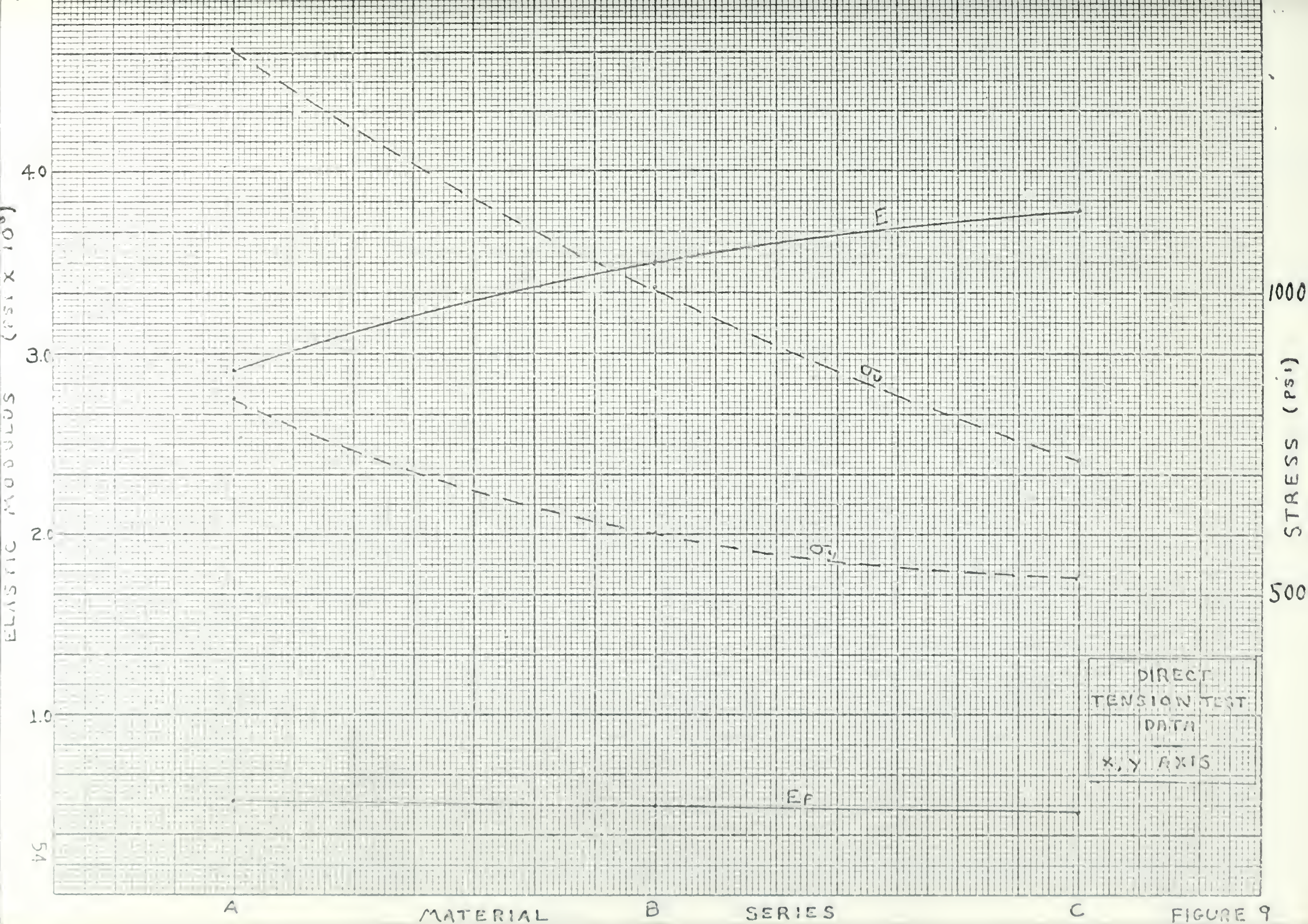
4.0
3.0
2.0
1.0
ELASTIC MODULUS (PSI X 10⁶)
1000
500
STRESS (PSI)
E
σ_u
σ_y
E_F
DIRECT
TENSION TEST
DATA
X, Y AXIS
A
MATERIAL
B
SERIES
C

FIGURE 9

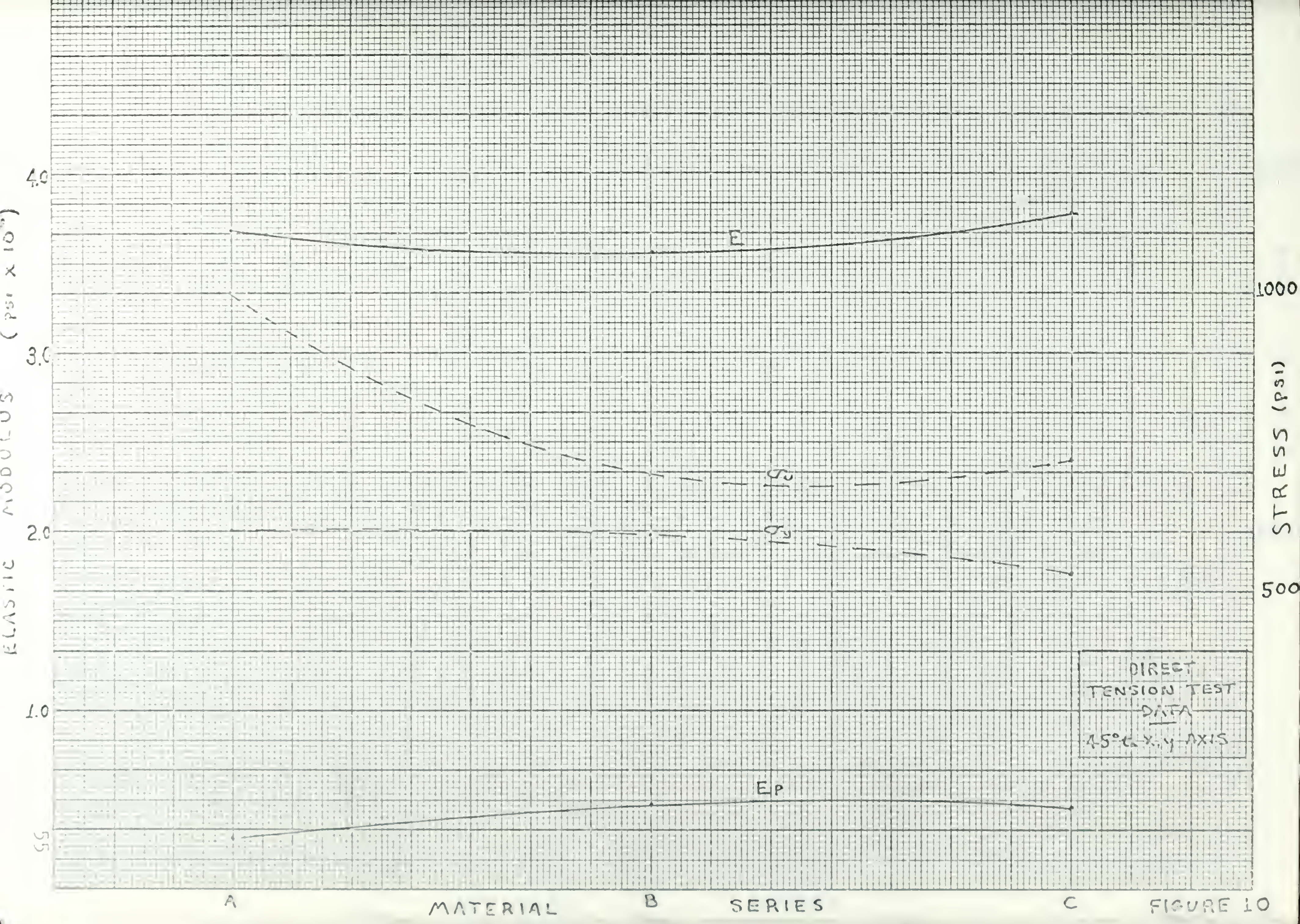
ELASTIC MODULUS (psi x 10)
4.0
3.0
2.0
1.0
55
STRESS (psi)
1000
500
E
σ_u
σ_y
Ep
DIRECT
TENSION TEST
DATA
45° to X, y AXIS
A
B
C
MATERIAL SERIES

FIGURE 10

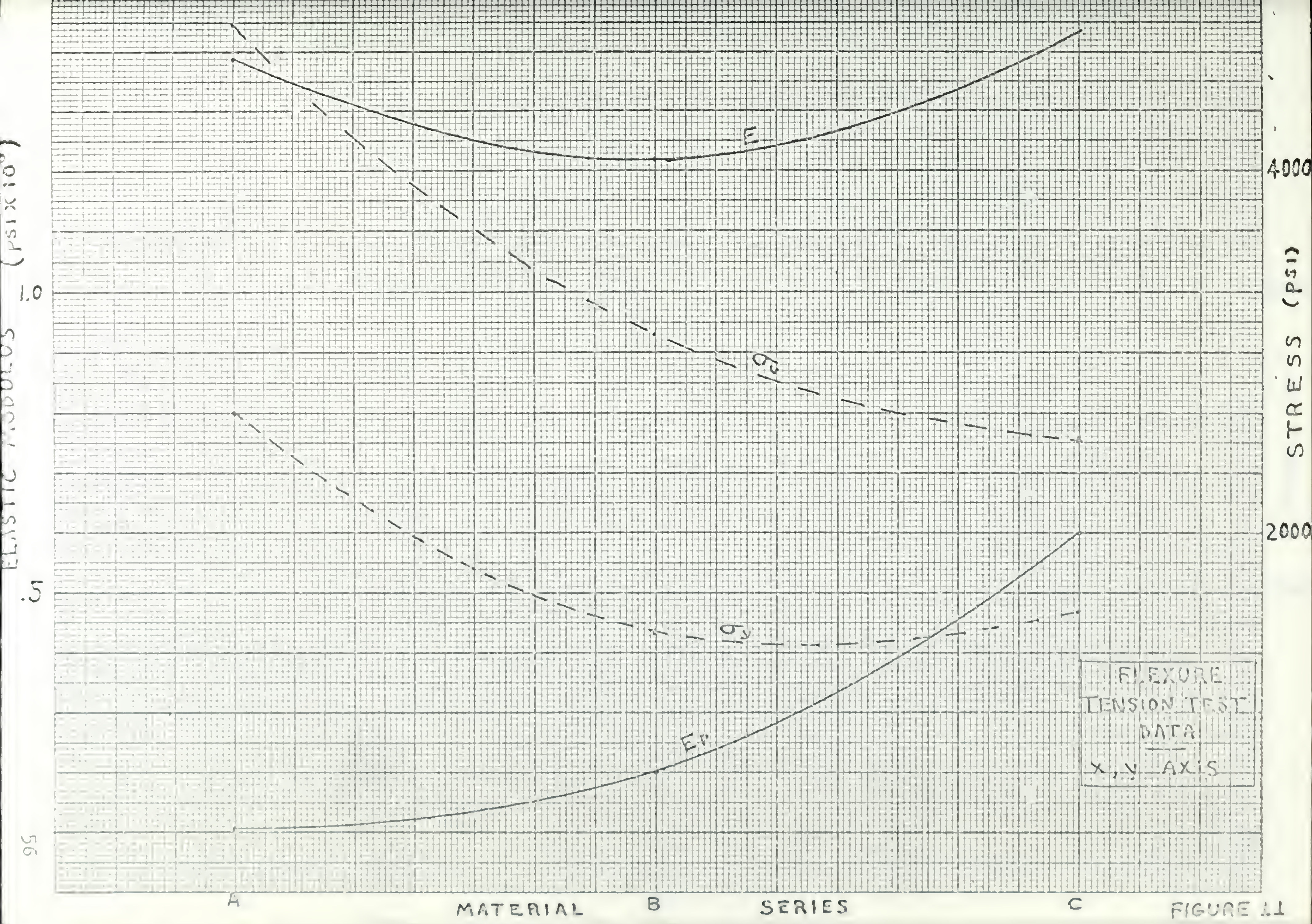
ELASTIC MODULUS (psi x 10⁶)
1.0
.5
STRESS (psi)
4000
2000
E
σ_u
σ_y
Ep
A
B
C
MATERIAL SERIES
FLEXURE
TENSION TEST
DATA
X, Y AXIS

FIGURE 11

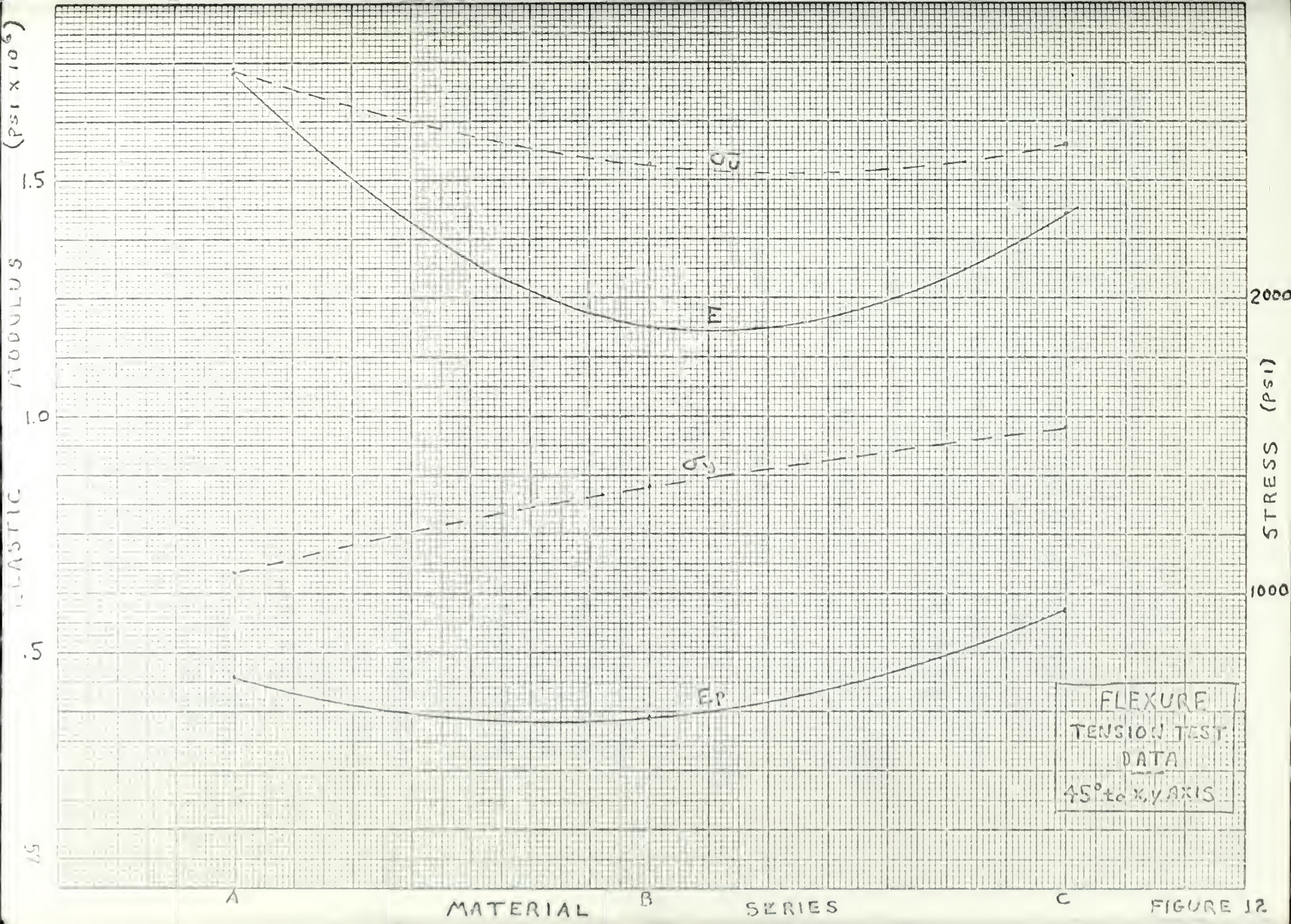
FLEXURE
TENSION TEST
DATA
45° to x,y AXIS
ELASTIC MODULUS (psi x 10⁶)
1.5
1.0
.5
STRESS (psi)
2000
1000
σ_u
E
σ_y
Ep
A
B
C
MATERIAL SERIES

FIGURE 12

Because the matrix does not deform plastically the stages of stress strain behavior of the composite reduces to:

1) elastic deformation of fiber and matrix
2) elastic deformation of fiber or pull out shear
3) plastic deformation of fiber or pull out shear

For continuous fiber reinforced composites the modulus for the first stage is given by:

$$E_c = E_f V_f + E_m V_m \tag{46}$$

and for the second and third stages:

$$E_c = E_f V_f \tag{47}$$

where E_f can be either the elastic or plastic modulus (for steel: $E = 30 \times 10^6$, $E_p = 10 \times 10^6$). The above formulae predict modululi as follows (using a modulus of 3.2×10^6 for the mortar) for parallel and randomly oriented fibers (using the factor .795 from (22)):

Stage	Ec: Parallel Oriented	Ec: Randomly Oriented
1	4.46×10^6 psi	3.56×10^6 psi
2	1.425×10^6	1.14×10^6
3	$.466 \times 10^6$	$.355 \times 10^6$

The modulus obtained in the tensile tests more closely agrees with stage 1. The modulus obtained in the flexure

test agrees with stage 2, and the plastic modulus found in both tests essentially agree with stage 3. The stress strain behavior for both continuous and discontinuous fiber reinforced composite is the same if the discontinuous fibers are longer than the critical length (34). It has been established that the random fibers of series B and C are shorter than the critical length yet the elastic modulus determined experimentally follows the continuous fiber relationship. Series C tests agree more closely than the other series with the above values. It can be hypothesized that earlier microcracking and undetectable stress relief in the unreinforced portion of the series A matrix causes an earlier transfer of load onto the continuous fibers thus presenting a slope somehwere between stage 1 and stage 2 which looks linear on the load deflection plot of test results.

The plastic modulus remains fairly constant for all forms of reinforcement. The low value for series A and B flexure tests is probably due to a sudden shift in the neutral axis and change in moment of inertia when the reinforcement assumes the load. As stated earlier this would cause the flexure formula to yield inaccurate results.

B. Material Properties 45° to x, y Axis

It was expected that the properties of all specimens in the 45° direction to the x or y axis would be enhanced with increased fiber content because of the random orient-

ation of the fibers (22). Regarding the elastic modulus and UTS the 45° specimens (fig. 10, 12) follow the results of the x, y specimens. In the tensile specimens (fig. 10), increased random fiber content and reduction of continuous reinforcement increases the elastic modulus and decreases the UTS, but the effect is less pronounced than in the x, y specimens. In the flexure specimens (fig.12) the elastic modulus decreases then increases and the UTS decreases with increased random fiber content. The expected result does occur with the yield strength and the plastic modulus except that yield strength in the tensile specimens decreases slightly.

C. Other Properties

1. Shear Strength

The shear strength obtained from the bending of a clamped beam is not a standard method of obtaining this quantity. However other tests such as the rotation between cylinder ends are not feasible when square mesh reinforcing is used. The failure mode of the clamped beam was definitely in shear, therefore the values obtained are used for purposes of the finite element analysis. These values however should not be interpreted as accurate values of shear stress for the material in general. Figure 13 shows shear strength decreasing as discontinuous fiber content increases and continuous fiber content decreases. This could be expected since the tensile yield stress was also

less for these specimens. However, substantial plastic shear work is done after yield in the specimens reinforced with random discontinuous fibers. Once the yield point in shear is reached in the mesh reinforced specimens abrupt unloading occurs. With the random fiber reinforced specimens the unloading occurs gradually after a period of continued deformation at the yield shear load. This result is also shown by cylinder compression tests. It is believed that this is the mechanism which causes the increased impact energy of the random fiber specimens (also plotted in figure 13) because the strain energy to be overcome by impulsive loading is greater. This strain energy was not measured since this was not the purpose of the paper.

2. Impact Energy

Figure 13 shows the increased impact energy per unit area for increased random discontinuous fiber content. These results were obtained in a standard Charpy test on a 260 ft-lb capacity Izod test machine. The potential energy and height of pendulum was the same for all tests. An increase of 103% in impact energy/unit area was obtained. All samples had the same steel content by weight and volume. As mentioned previously the increased strain energy noted in the shear and compressive cylinder tests accounts for the increased impact energy found in this test.

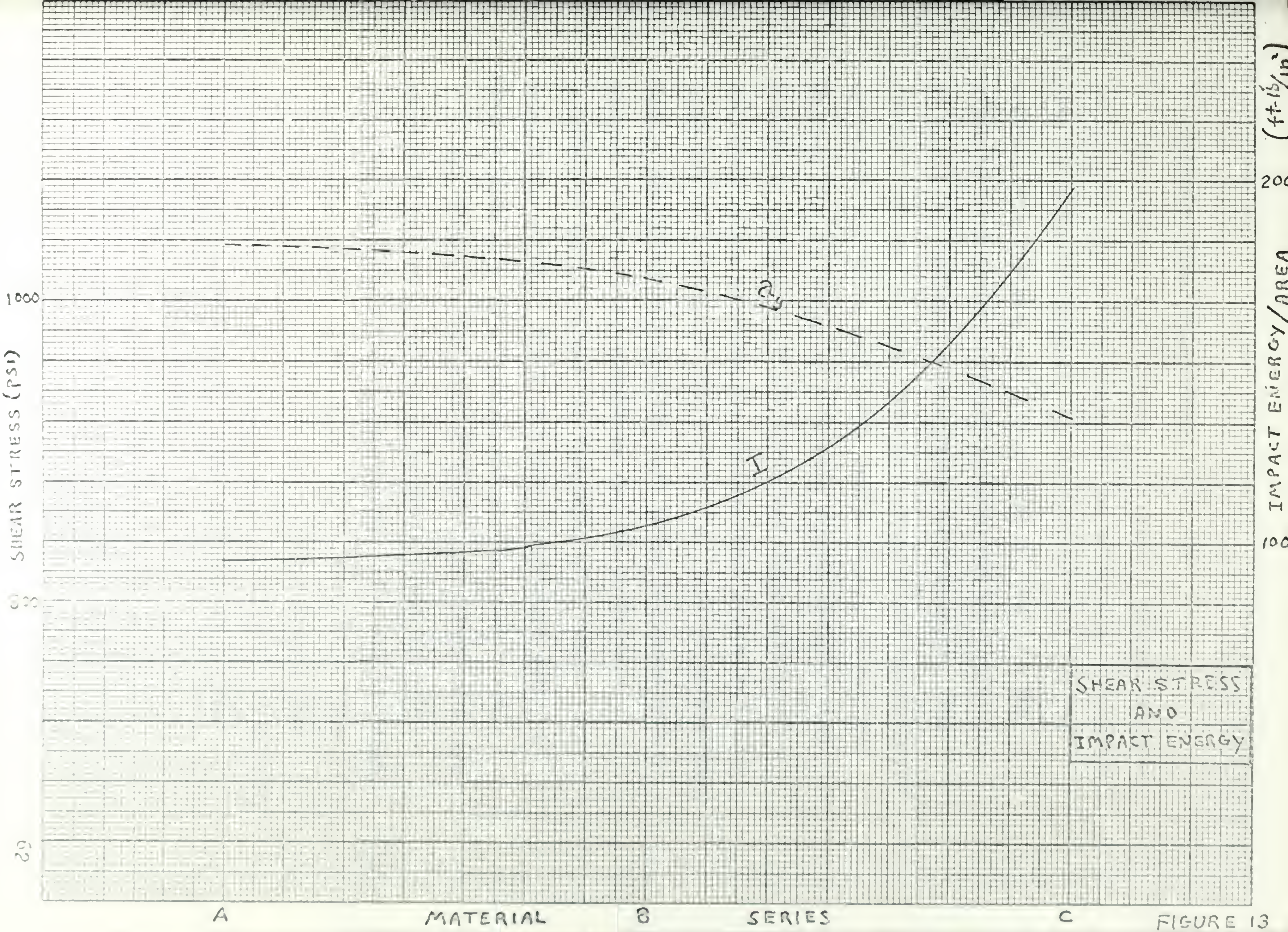

SHEAR STRESS AND IMPACT ENERGY

FIGURE 13

D. Cylinder Compression Tests (fig. 14)

The cylinder compression tests show a marked increase in ultimate compression strength and modulus of elasticity with inclusion of fibers. An increase of 19.7% in the modulus of elasticity and an increase of 24.3% in the ultimate compression strength is obtained for inclusion of 4.75% (by volume) random fiber reinforcement. The mode of failure is quite different between the unreinforced cylinders and those containing random fibers (figure 22). Whereas the unreinforced cylinders failed abruptly with immediate relaxation of the load, the fiber reinforced cylinders after reaching the failure load maintained this load for an additional .004 strain (or .012" of deformation) before gradually relaxing the load under increased deformation. The failure mechanisms for the 4.75% fiber reinforced cylinders was the formation of an upset (bulge) around the middle. The 2.37% fiber reinforced cylinders failed partially by splitting and partially by upset.

The fibers in the case of impact and compression are evidently not being subjected to shear along the bond interface as in the tension tests, but are being subjected to stresses normal to the fiber matrix interface. The fibers are attempting to hold the matrix together in a direction normal to the fiber axis, e.g. they act to prevent the splitting action which is the failure mode of the unreinforced mortar cylinders.

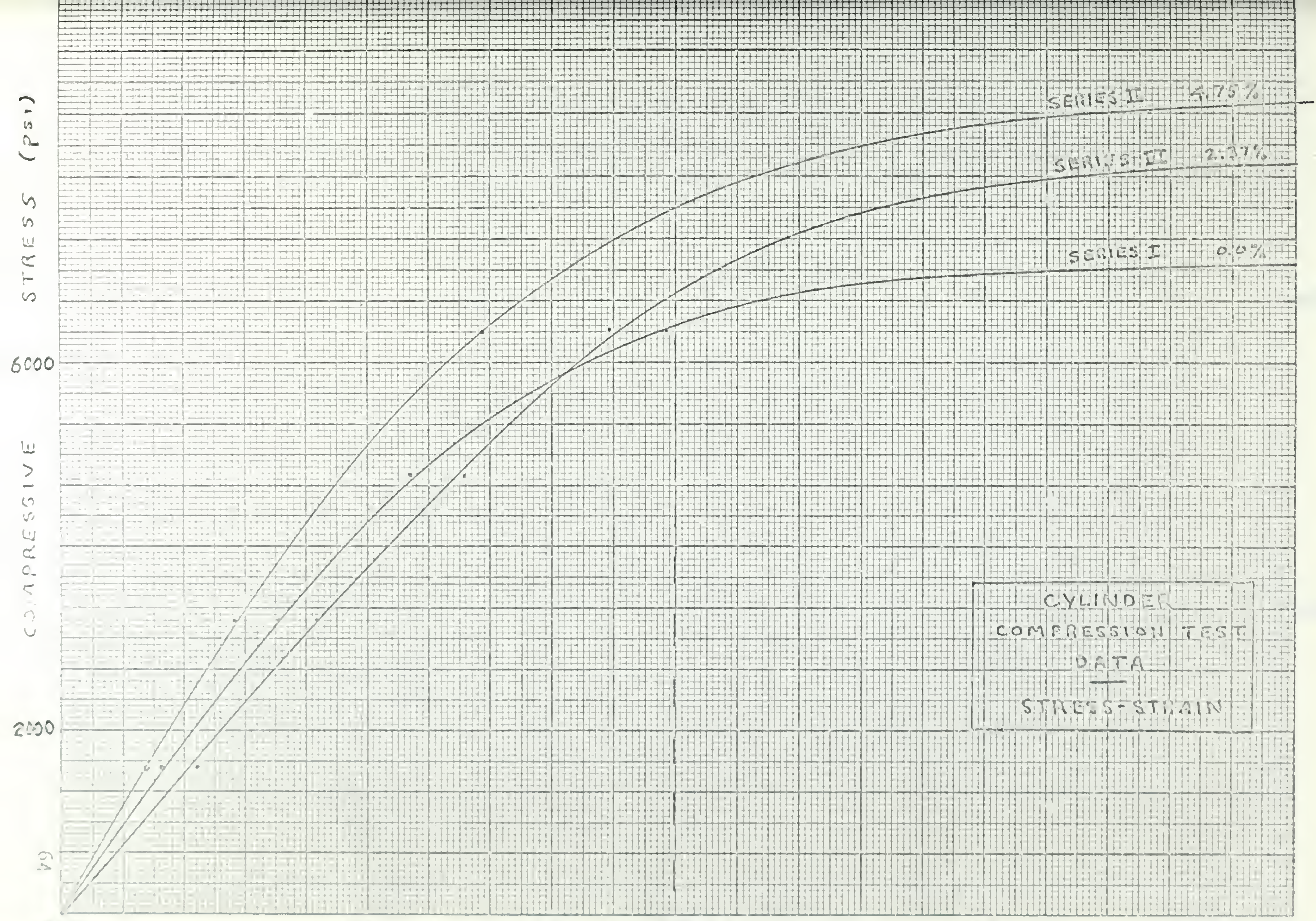
CYLINDER
COMPRESSION TEST
DATA
STRESS-STRAIN
SERIES II 4.75%
SERIES III 2.37%
SERIES I 0.0%
COMPRESSIVE STRESS (psi)
6000
2000
0
STRAIN (in/in)
0
.001
.002
.003

FIGURE 14

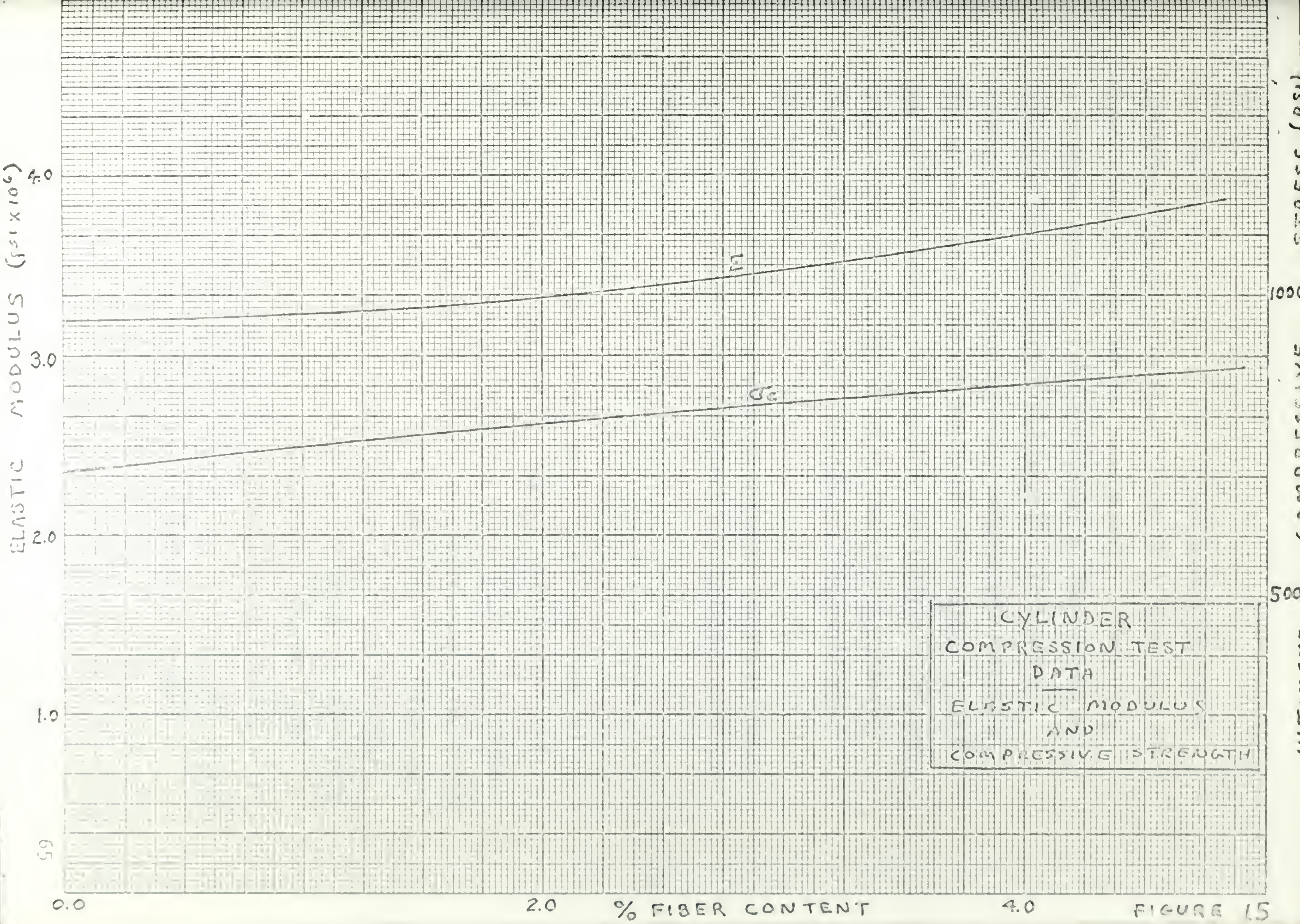
ELASTIC MODULUS (psi x 10⁶)
4.0
3.0
2.0
1.0
0.0
2.0
4.0
% FIBER CONTENT
1000
500
E
σc
CYLINDER
COMPRESSION TEST
DATA
ELASTIC MODULUS
AND
COMPRESSIVE STRENGTH

FIGURE 15

The secant modulus for the 4.75% fiber reinforced specimens does not agree exactly with that found with the direct tension tests for the same material. This is to be expected because of the difference in the methods of obtaining the respective yield points. The important finding is that in both cases the modulus of elasticity is increased over that of the mortar (in tension by 17.9% and in the compression by 19.7%) by the inclusion of random fibers which have an ℓ/d far less than the theoretical critical ℓ_c/d required for enhancement of properties of the composite.

These results also agree in principle with the theory of Romualdi regarding the mechanism for enhancing fracture toughness.

E. Plate Bending

The failure mode of each plate series was local at the area of load application. The mesh reinforced specimens deformed in a mound much as a steel plate would deform. The random fiber plates deformed in a tent shape along local yield lines (fig. 21, 23). Due to the form of loading some punching effect occured at the surface where the load was applied. This manifested itself as a crushing of the mortar out to a .45" radius and to a mean depth of .058". This crushing action commenced upon application of the load. Delamination of the surface mortar down to this depth occured when ultimate plate bending was reached which indicates

that this portion of the plate did not contribute to the resistance of load during plate bending. Typical failed specimens are shown in figure 23.

Figure 16 shows the plot of load-deflection for each plate series normalized on the basis of the cube of equivalent thickness ratio. This figure indicates that the random fiber reinforcement increases ultimate bending load and deflection. The combination of random fiber and continuous fiber reinforcement in equal proportions yields an even greater increase in bending ultimate strength and deflection as well as allowing for some resistance to membrane stress after ultimate bending failure (fig. 17). With the proper combination of random fibers and continuous mesh a design point can be reached which will yield the optimum in either ultimate bending strength or membrane effect after bending failure.

The prediction of the membrane effect was not attempted in the finite element analysis. From figure 17 however, it is clearly a function of the amount of continuous fiber reinforcement in the material. The slope of the curves in the membrane region are:

$$\text{Series A} = \frac{315}{.2} = 1575 \text{ lb/in}$$

$$\text{Series B} = \frac{155}{.2} = 775 \text{ lb/in}$$

This ia a 2:1 relation within experimental error. The amount of mesh reinforcement in the two series is also in a 2:1 porportion. Thus, for this type of loading condition, if an

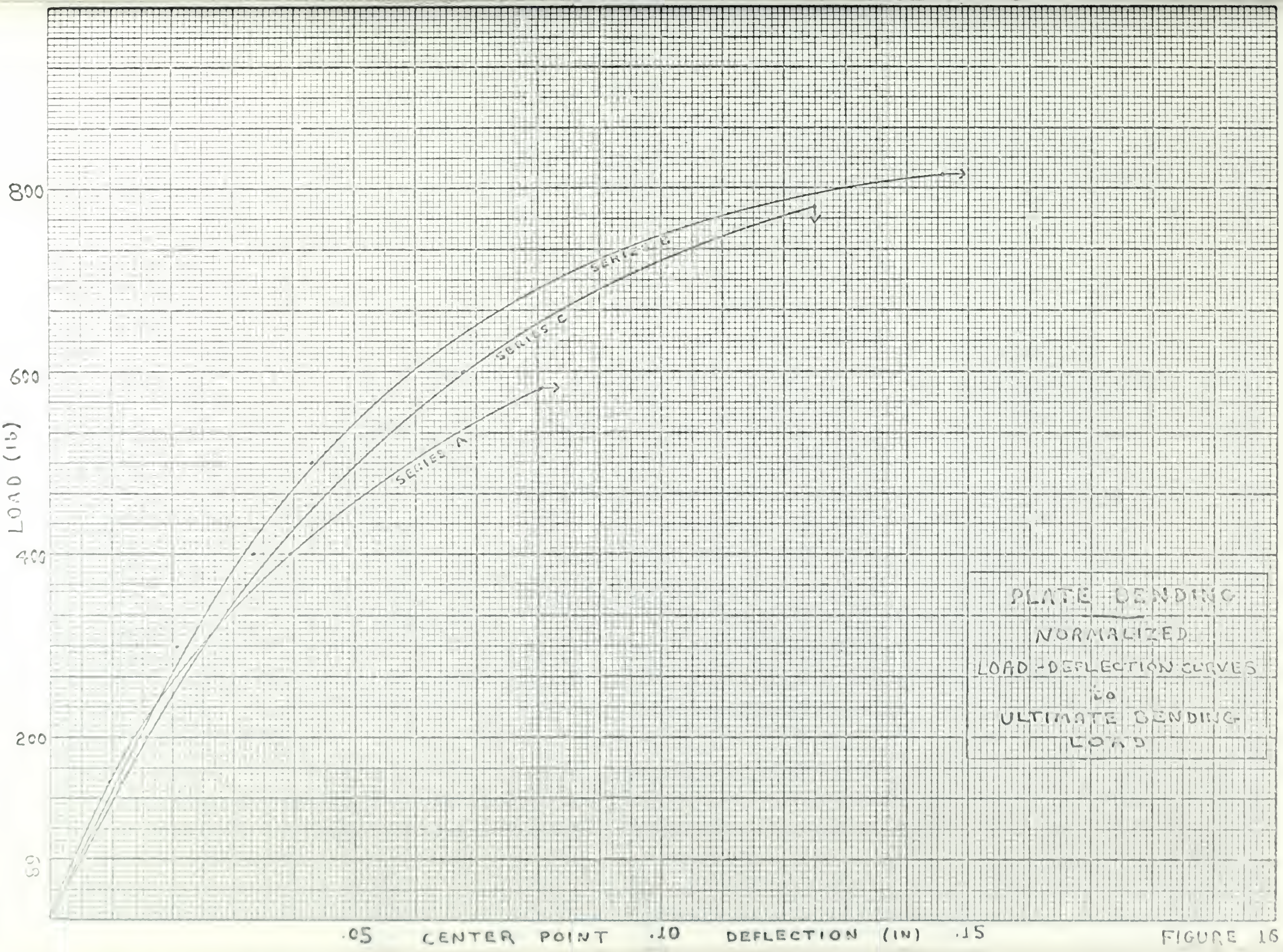PLATE BENDING
NORMALIZED
LOAD-DEFLECTION CURVES
to
ULTIMATE BENDING
LOAD
SERIES A
SERIES C
SERIES B
800
600
400
200
LOAD (lb)
.05
.10
.15
CENTER POINT DEFLECTION (IN)

FIGURE 16

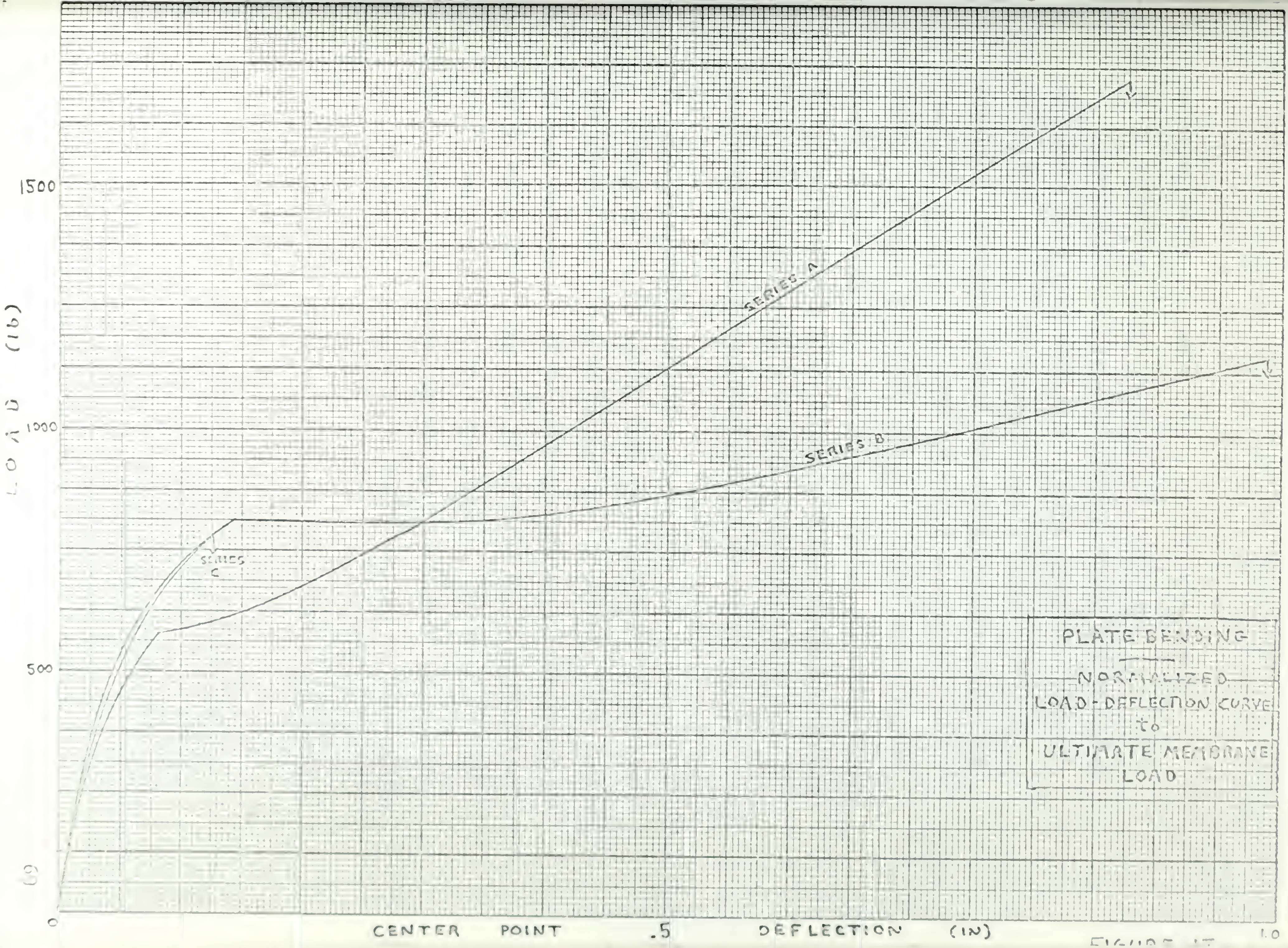
PLATE BENDING
NORMALIZED
LOAD-DEFLECTION CURVE
to
ULTIMATE MEMBRANE
LOAD
SERIES A
SERIES B
SERIES C
LOAD (lb)
1500
1000
500
0
CENTER POINT DEFLECTION (IN)
.5
1.0

FIGURE 17

engineer wishes to design for a specified membrane ultimate load a direct relation is indicated.

Returning to figure 16, the properties determined in the first part are consistent with the results. Better properties in the 45^{0} direction and a higher modulus obtained with random fibers increases the area under the load deflection curve. The lower yield strength of series C (random fiber) is offset by these improvements. Series B shows that an optimum combination of random fibers and continuous mesh that possesses higher ultimate bending load and strain energy than either the individual mesh or randon fiber reinforced materials is possible.

F. Finite Element Analysis

Figures 18, 19 and 20 show the comparison of experimental center point load-deflection to the output of the finite element orthotropic plate bending computer program developed by B. Whang (29). Appendix II contains the significant input and output data from the program. The thickness of the plates were reduced by the amount of .058" to account for the non-contributory plate thickness due to delamination of a protion of the surface morter. This value of the thickness of the delaminated protion was determined using a depth micrometer.

Agreement is very good between the predicted and experimental load deflection curve for series B. This indicates that it is feasible to use this program with

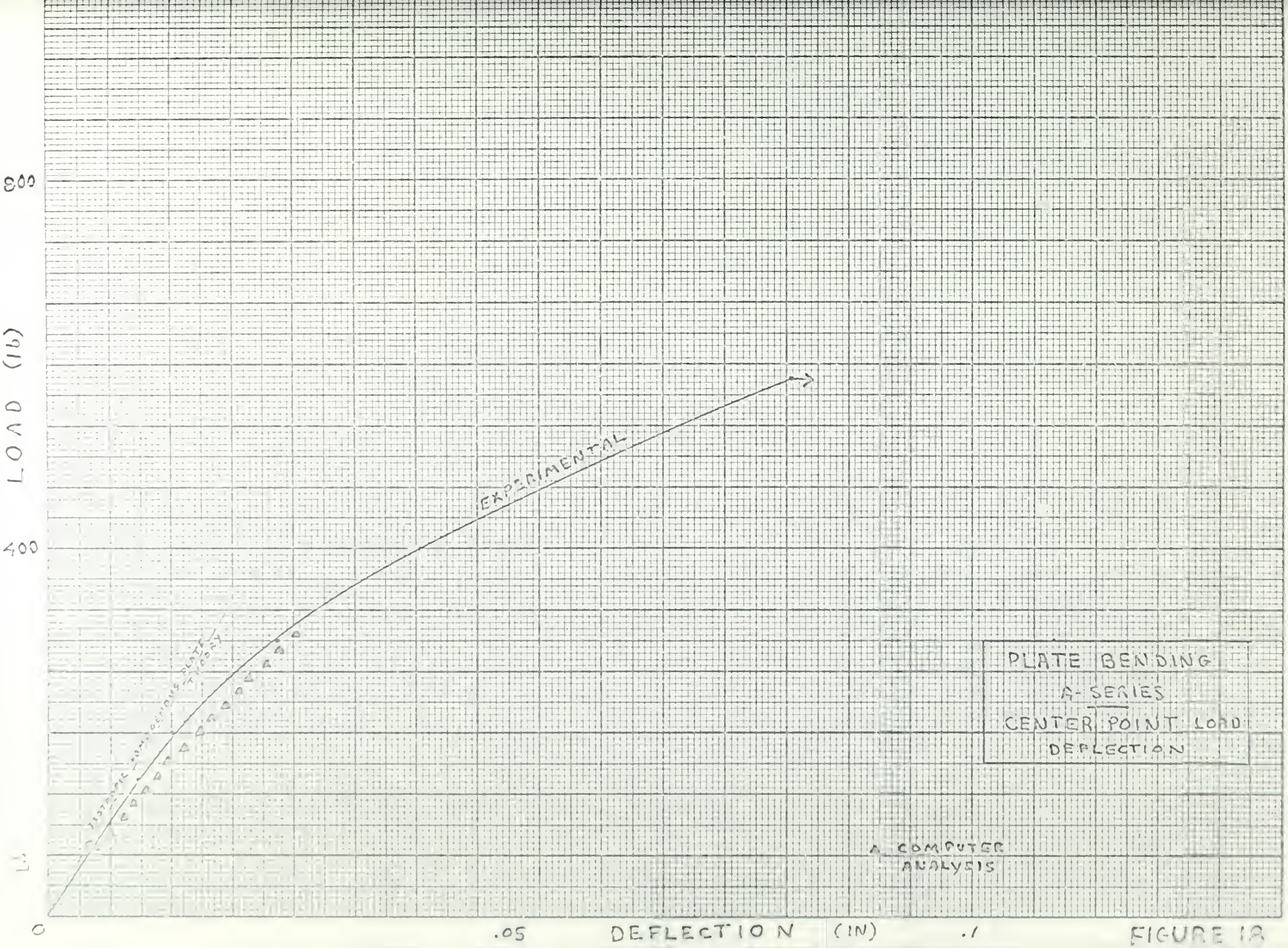
800
LOAD (lb)
400
0
.05
DEFLECTION (IN)
.1
EXPERIMENTAL
ISOTROPIC HOMOGENEOUS PLATE THEORY
PLATE BENDING
A-SERIES
CENTER POINT LOAD
DEFLECTION
Δ COMPUTER ANALYSIS

FIGURE 18

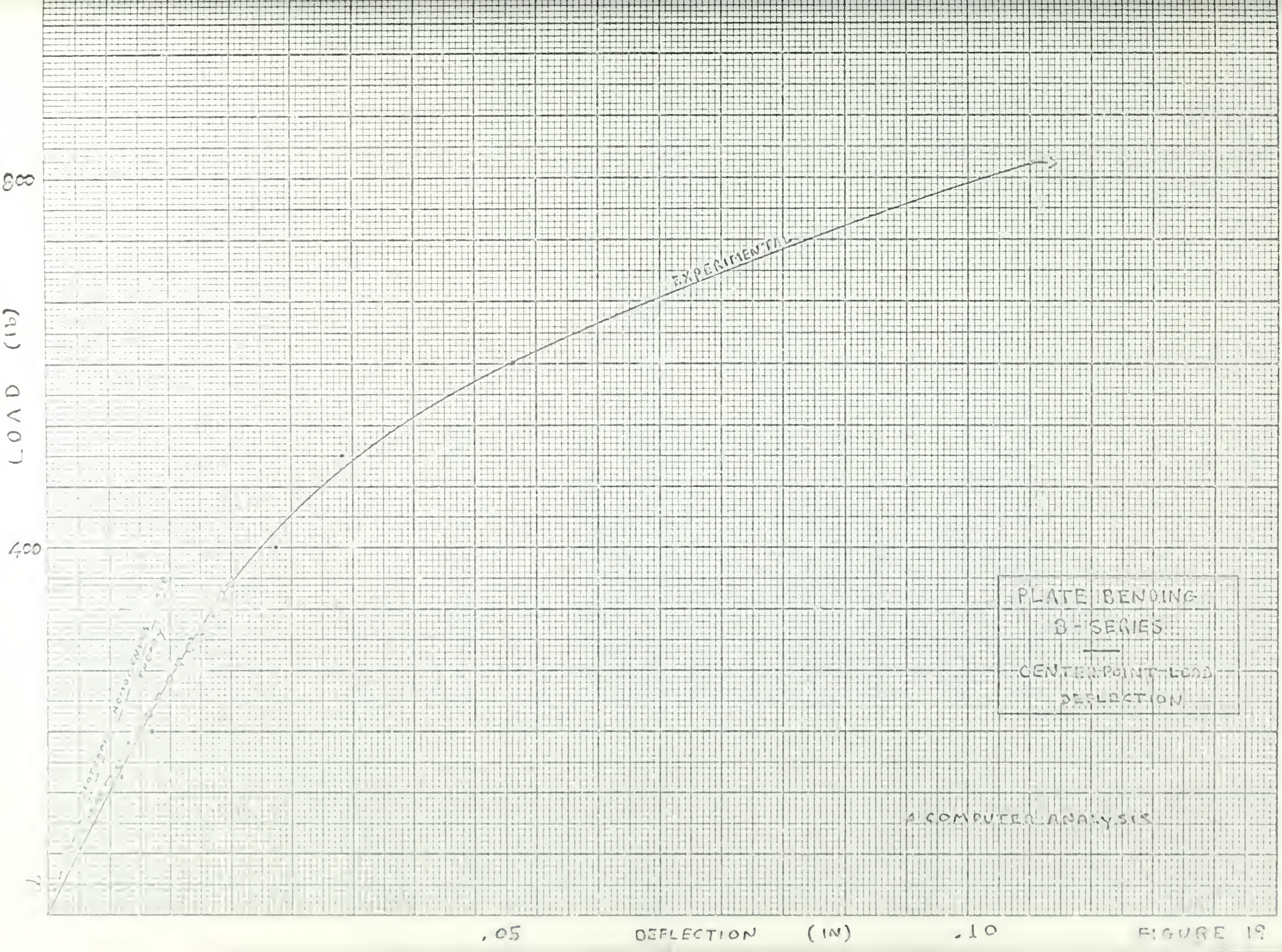

PLATE BENDING
B-SERIES

CENTER-POINT LOAD
DEFLECTION

FIGURE 19

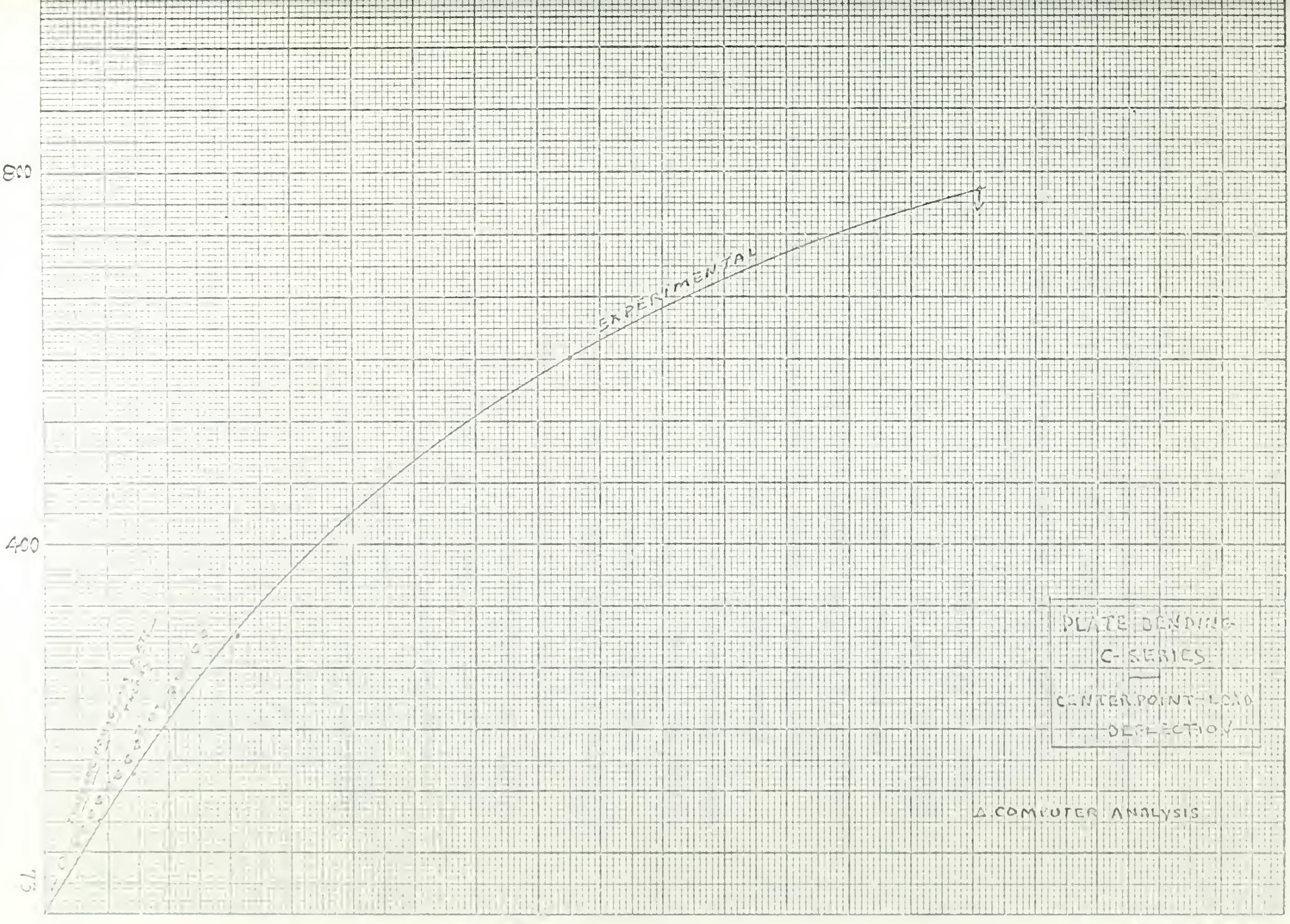
800
400
73
.05
.1
EXPERIMENTAL
PLATE BENDING
C-SERIES
CENTER POINT LOAD
DEFLECTION
Δ COMPUTER ANALYSIS

FIGURE 20

input of experimental data to predict the behavior of ferro-cement plates well into the plastic bending region. The condition of loading in this case causes the additional variable of delamination of surface unreinforced mortar. It would be expected that under a uniform plate loading good results would also be obtained without the delamination problem. Agreement is fair for series C and series A. The program predictes greater deflections for the mesh reinforced series (maximum error 19.3%) and smaller deflections for the short random fiber reinforced series (maximum error -17.6%) from those obtained experimentally. This disparity could be due to variation of the thickness of the delaminated portion of the plates between series, thus changing the value of the actual contributory plate thickness. The value .058" represents an average over all the plates for the depth of crushing at the load point. The series A prediction indicates a tendency to agree closely with the experimental data as it progresses up the load deflection curve whereas the series C prediction diverges with increasing load. It would appear that the program would diverge from experimental results as ultimate plate bending load is approached.

The finite element analysis used here is very sensitive to the incremental increase in load for each iteration in the plastic range. Incremental loads less than 20 lb at each element should be used in order to avoid divergence by the program. The program is capable of accepting data

for any rectangular geometry and loading condition and provides for element thickness variation and curvature. It has been recently modified by Whang to accept layered material properties so that treatment of a composite using the individual material properties is now possible.

The yield load and maximum load deflection curve predicted by homogeneous isotropic plate theory for the elastic range is computed for each series in Appendix III. These values are plotted in figures 18, 19 and 20 to show the variation from homogeneous isotropic plate theory of the finite element plot and the experimental results.

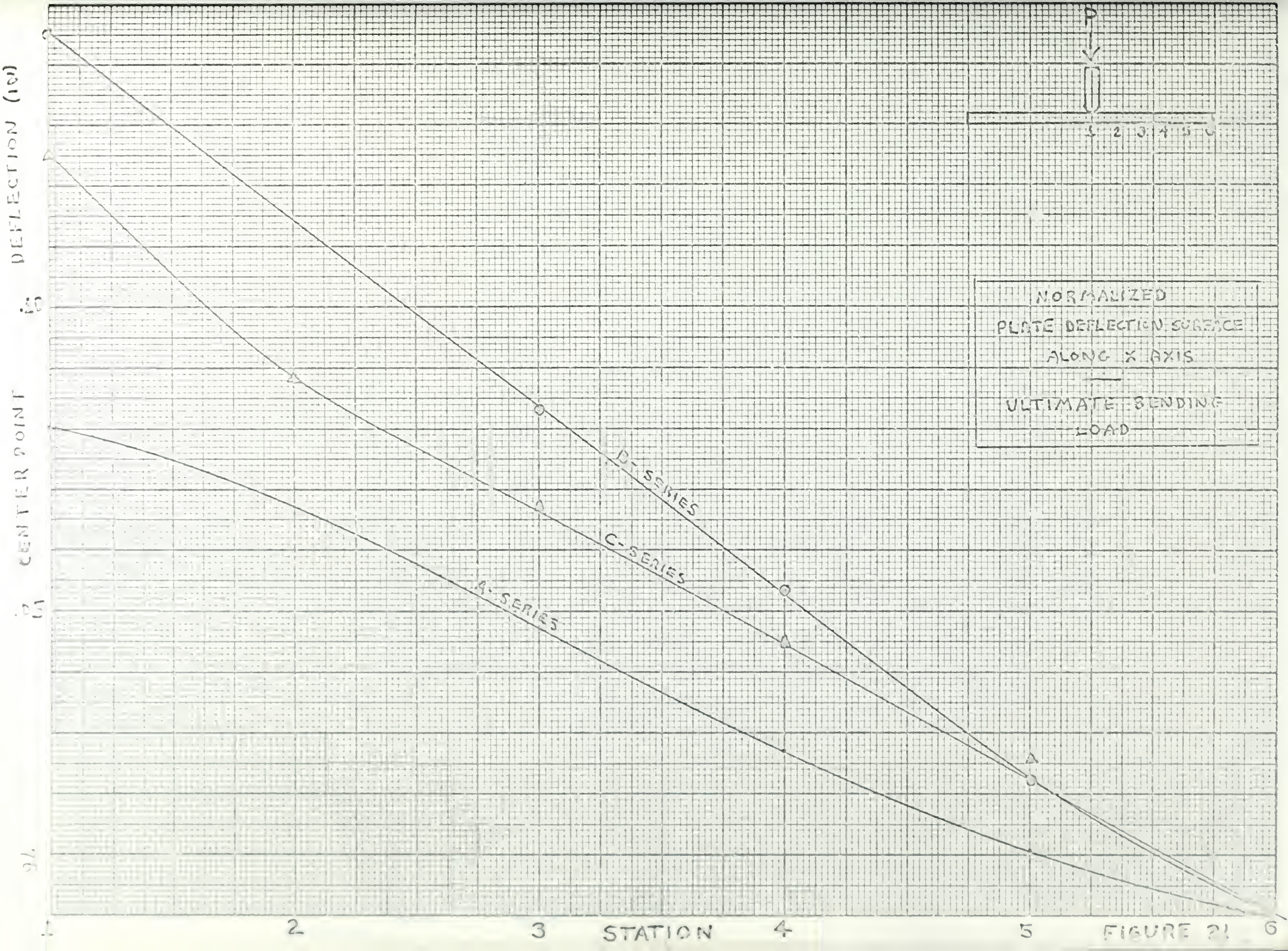
P
1 2 3 4 5 6
NORMALIZED
PLATE DEFLECTION SURFACE
ALONG X AXIS
ULTIMATE BENDING
LOAD
B-SERIES
C-SERIES
A-SERIES
CENTER POINT DEFLECTION (IN)
.75
.50
76
1
2
3
4
5
6
STATION

FIGURE 21

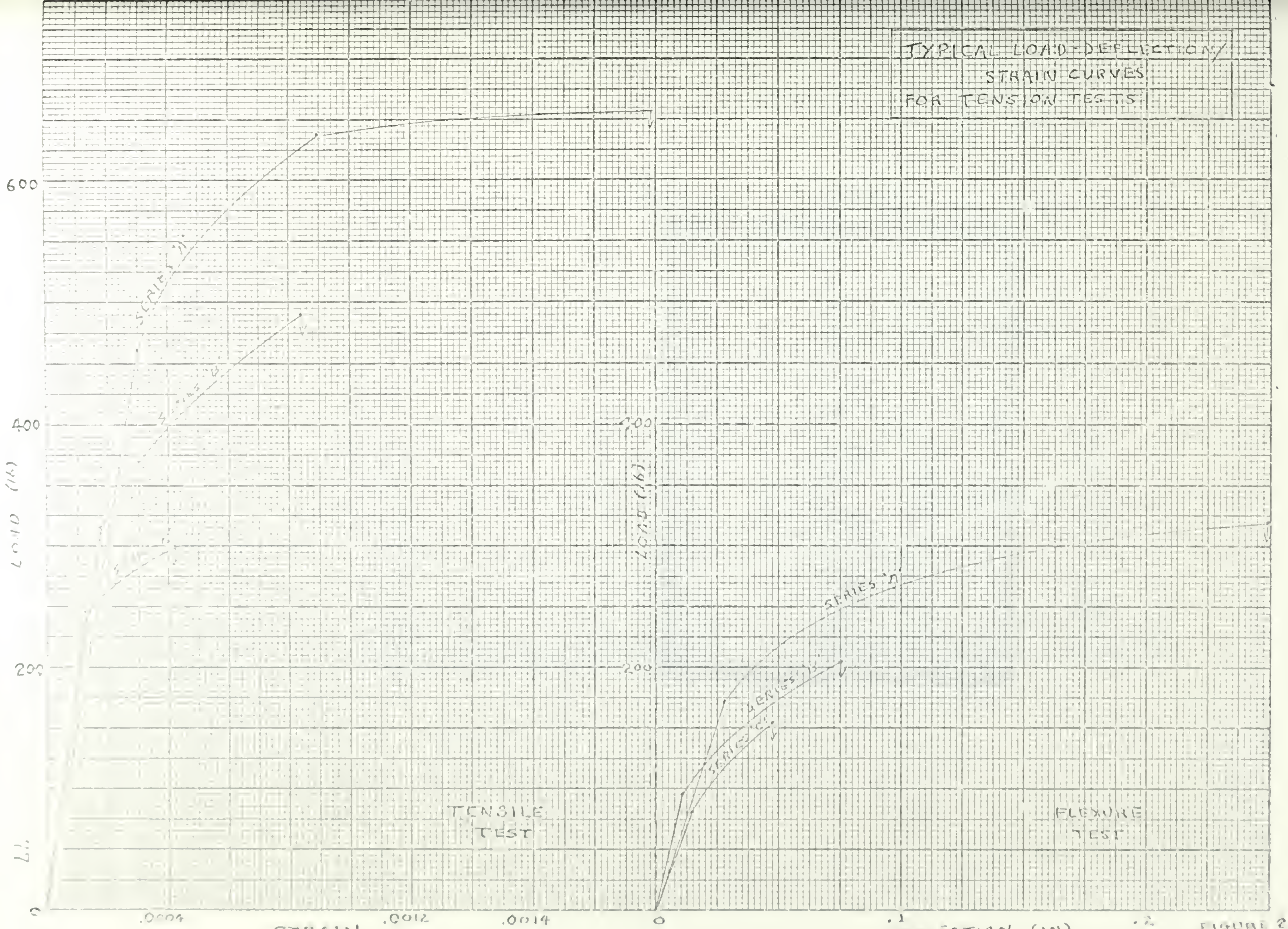
TYPICAL LOAD-DEFLECTION/
STRAIN CURVES
FOR TENSION TESTS
600
400
200
0
LOAD (lb)
LOAD (lb)
200
200
SERIES 'A'
SERIES 'B'
SERIES 'C'
SERIES 'A'
SERIES 'B'
TENSILE TEST
FLEXURE TEST
.0004
.0012
.0014
0
STRAIN
.1
.2
DEFLECTION (IN)

FIGURE 2

Compression Cylinders After Ultimate Failure

Figure 22

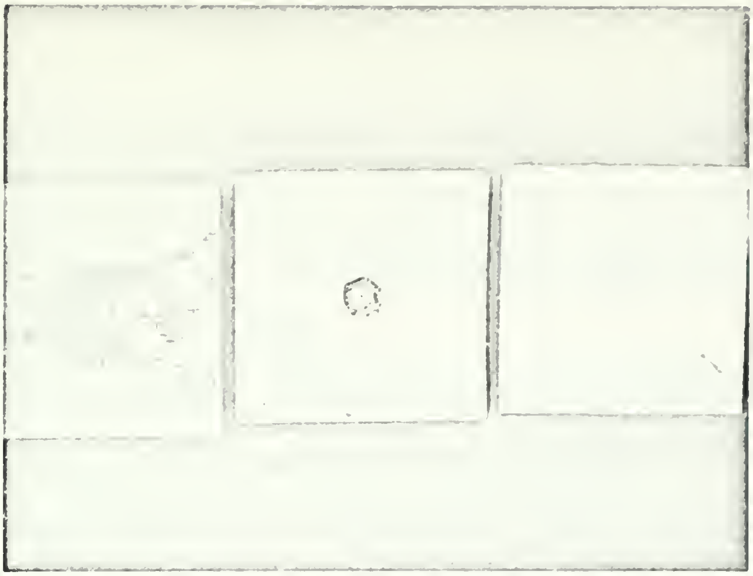

Compression Face

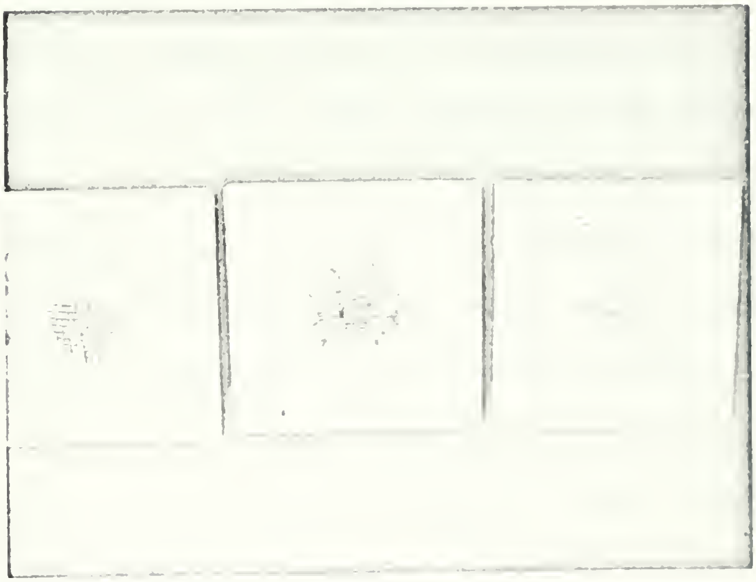

Tension Face

Figure 23 Plate Specimens After Ultimate Failure

VI CONCLUSIONS

Based on the experimental results and their broad agreement with theoretical predictions the following conclusions regarding the engineering properties of ferro-cement may be made:

a) Short random fibers with $l < lc$ enchance compressive strength and modulus of elasticity of cement mortar.

b) Replacement of continuous fiber reinforcement with short random fibers increases the elastic modulus but decreases the ultimate and yield tensile stresses of ferro-cement.

c) Random fibers with $l < lc$ enhance the modulus of elasticity and yield stress in the axis 45° to the x, y axis in mesh reinforced mortar.

d) Random fibers with $l < lc$ increase the plastic work of deformation in shear and compression tests.

e) Impact energy/area is greatly enhanced over that of mesh reinforced mortar of the same steel content by inclusion of short random fibers.

Bending of ferro-cement plates for the particular loading condition used in this thesis may be closely predicted by the finite element analysis developed by Whang for orthotropic plates providing the correct properties of the particular type of ferro-cement are used. In general

the replacement of continuous mesh reinforcement with short random fibers in ferro-cement plates results in:

a) Increased ultimate plate bending load.

b) Decreased ultimate plate membrane load.

c) Increase in plastic work done in deforming the plate.

The slope of the membrane load deflection curve for a ferro-cement plate varies directly as the percent content by weight of continuous wire reinforcement for the particular loading situation considered in this thesis.

VII RECOMMENDATIONS

The following areas need further clarification:

a) Deformation of ferro-cement plates under uniform loading.

b) The mechanism of fracture when continuous mesh is used as reinforcement since the measured modulus of elasticity did not agree with that of theory.

c) The mechanism of plate work in the deformation of random fiber reinforced mortar.

VIII REFERENCES

1. Tuthill, L.H. "Concrete Operations In The Concrete Ship Program" Proc. ACI V. 41 (1945) pp. 137-180
2. Watstein, D "Effect of Straining Rate On The Compressive Strength & Elastic Properties of Concrete" Proc. ACI V.49 (1953) pp. 729-744
3. Eringen, A.C. "Transverse Impact On Beams & Plates" J. Appl. Mech. V.20 (1953) pp. 461
4. Irwin, G.R. "Analysis of Stresses & Strains Near The End of A Crack Transversing A Plate" J.Appl. Mech. V. 24 (1957) pp. 361
5. Greaves, M.J. Mavis, F.T. "Inelastic Behavior of Impulsively Loaded Beams" Proc. ASCE Stru. Div. Journal V. 83 ST 3 May 1957 pp. 1232
6. Collen, L.D.G. Kirwan, R.W. "Some Notes On The Characteristics of Ferro-Cement" Civil. Eng. & Public Works Review Feb. 1959 pp. 195-196
7. Cox, A.D. Morland, L.W. "Dynamic Plastic Deformation Of Simply Supported Square Plates" J. Mech. Phys. Solids V.7 1959 pp. 229-241
8. Collen. L.D.G. "Some Experiments in Design and Construction With Ferro-Cement" The Institution of Civil Engineering of Ireland, paper presented at 4 Jan. 1960 general meeting.

9. Romualdi, J.P. Batson, G.B. "Mechanics of Crack Arrest In Concrete" Proc. ASCE V. 89 EM 3 June 1963 pp. 147-168

10. Romualdi, J.P. Batson, G.B. "The Behavior of Reinforced Concrete Beams With Closely Spaced Reinforcement" ACI Journal PROC V. 60 #6 June 1963 pp.775-789

11. Romualdi, J.P. Mandel, J.A. "Tensile Strength Of Concrete Affected By Uniformly Distributed & Closely Spaced Short Lengths Of Wire Reinforcement" ACI Journal V. 61 #6 June 1964 pp. 657-672

12. Green, H. "Impact Strength Of Concrete" Proc. The Institute of Civil Eng. (London) V. 28 June 1964 pp. 383

13. Nawy, E.G. "Flexural Cracking In Two-Way Concrete Slabs Reinforced With High Strength Welded Wire Fabric" ACI Proc. V. 61 Aug. 1964 pp. 997-1008

14. Williamson, G.R. "Fibrous Reinforcement For Portland Cement Concrete" Tech. Rept. #2-40 May 1965 U.S. Army Eng. Div. Corp of Eng. Ohio River Div. Lab.

15. Bajan, R.L, Jr. "Strength of Fiber Reinforced Concrete With Aggregate" CE MS Thesis Clarkson College of Tech. June 1965

16. Jacobsen, A. "Membrane Flexural Failure Modes Of Square Horozontally Restrained R/C Slabs" MIT CE ScD Thesis 1965

17. Romualdi, J.P. Ramey, M.R. "Effect Of Impulsive Loads

On Fiber Reinforced Concrete Beams" Final Report Dept. of C.E. Carnegie Inst. of Tech. Pittsburg Oct. 1965 (Access Nr. AD 630-343)

18. Romualdi, J.P. Ramey, M.R. Sanday, S.C. "Prevention And Control Of Cracking By Use Of Short Random Fibers" ACI Publication SP-20 Paper #10

19. Williamson, G,R. "Response Of Fibrous-Reinforced Concrete To Explosive Loading" Tech. Rept. #2-48 Jan. 1966 U.S. Army Eng. Div. Corps of Eng. Ohio River Div. Lab.

20. Goldsmith, W. Polivka, M. Yang, T. "Dynamic Behavior Of Concrete" Experimental Mechanics V. 6 #2 1966 pp. 65

21. Bailey, L.E. "Fatigue Strength Of Steel Fiber Reinforced Concrete" CE MS Thesis Clarkson College of Tech. Oct.1966

22. Nielsen, L.E. Chen, P.E. "Young's Modulus Of Composites Filled With Randomly Oriented Fibers" Journal of Materials V.3 #2 June 1968 pp.352-358

23. Goldsmith, W. Kenner, V.H. Ricketts, T.E. "Dynamic Loading Of Several Concrete-Like Mixtures" ASCE Proc. Struct. Div. V. 94 ST7 July 1968 pp.1803-1827

24. Moavenzadeh, F. Kuguel, R. Keat, L.B. "Fracture of Concrete" Dept. of CE. MIT Rept. #R68-8 March 1968

25. Kelly, A.M. Mouat, T.W. "Ferro-Cement As A Fishing Vessel Construction Material" Conf. on Fishing

Vessel Construction Materials Oct. 1-3 1968 Montreal Canada Federal Provencial Atlantic Fishing

26. Collins, J.F. "Tensile Strength Of Mesh Reinforced Mortar" Unpublished Term Report May 7, 1968 CE Dept. MIT

27. McKenny, J.L. "Tensile Strength Of Steel Fiber Reinforced Concrete" CE MS Thesis, Clarkson College of Technology May 1964

28. Collins, J.F. Claman, J.S. "Ferro-Cement For Marine Applications-An Engineering Evaluation" Paper presented before the Mar. 7 1969 meeting of the New England Section of SNAME

29. Wang, B. "Elasto-Plastic Analysis Of Orthotropic Plates And Shells" Research Report R-68-83 CE Dept. MIT

30. Griffith, A.A. "Theory Of Rupture" Proc. 1st. International Cong. for Applied Mechanics pp. 55-63 1924

31. Jayne, B.A. Suddarth, S.K. "Matrix-Tensor Mathematics In Orthotropic Elasticity" Orientation Effects In The Mechanical Behavior Of Anisotropic Structural Materials ASTM STP 405 1966 pp. 39

32. Timoshenko, S. *Theory Of Plates And Shells* McGraw Hill 1959

33. Huber, M.T. *Probleme der Statik Technisch Wichtiger*

Orthotroper Platten Warszawa 1929

34. Kelly, A. Davies, G.J. "The Principles Of The Fiber Reinforcement Of Metals" Metallurgical Reviews 1965 V. 10 No. 37

35. Alexander, K.M. "The Mechanism Of Shear Failure At The Steel-Cement And Aggregate-Cement Interface" International Conference on Structure, Solid Mechanics and Engineering Design In Civil Engineering Materials, University of Southampton 21-25 April 1969

36. Troxell & Davis _Composition And Properties Of Concrete_ McGraw-Hill 1956

APPENDIX IA

Experimental Results: A-Series (42 mil steel mesh reinforced mortar)

Tensile Tests
x, y Direction

Spec	b	h	P_y	P_u	ϵ_y	ϵ_u	σ_y	E	σ_u	E_p
A-1	.95	.46	460	660	.00036	.0014	1052	2.92	1510	.414
A-2	.92	.45	360	640	.0004	.0012	870	2.18	1545	.845
A-3	.98	.45	420	680	.0003	.0012	954	3.17	1540	.586
A-4	.97	.48	410	650	.0003	.0019	880	2.93	1394	.321
A-5	.97	.48	510	670	.00036	.00316	1095	3.04	1440	.123
A-6	.96	.43	200	640	.00016	.0026	485	3.03	1550	.435
A-7	.95	.45	340	600	.00024	.00144	795	3.06	1405	.508
A-8	.96	.49	240	610	.00017	.001	510	3.0	1300	.930
					Average		830	2.91	1460	.52

45° to x, y Direction

Spec	b	h	P_y	P_u	ϵ_y	ϵ_u	σ_y	E	σ_u	E_p
A-1	.98	.46	300	430	.00016	.0012	666	4.16	950	.273
A-2	.96	.43	190	430	.00012	.0016	450	3.84	1040	.4
A-3	.94	.42	265	370	.00012	.00144	671	5.6	936	.2
A-4	.97	.43	260	440	.00020	.002	623	3.11	1055	.237
A-5	.90	.44	230	410	.00034	.002	582	1.71	1035	.273
					Average		598	3.68	1003	.276

Flexure Tests
45° to x, y Direction

Spec	b	h	P_y	P_u	δ_y	δ_u	σ_y	E	σ_u	E_p
A-1	.95	.47	40	115	.006	.04	930	1.92	2675	.65
A-2	.97	.44	42	112	.008	.07	1090	1.81	2905	.388
A-3	.985	.44	44	116	.009	.07	1125	1.65	2965	.4
A-4	.97	.475	51	116	.009	.06	1135	1.56	2585	.350
					Average		1070	1.73	2780	.448

x, y Direction

Spec	b	h	P_y	P_u	δ_y	δ_u	σ_y	E	σ_u	E_p
A-1	1.05	.45	103	205	.03	.332	2480	1.07	4700	.095
A-2	1.05	.44	113	156	.02	.18	2710	1.79	3740	.085
A-3	1.0	.5	170	320	.028	.256	3300	1.37	6240	.151
A-4	1.0	.46	100	195	.022	.38	2300	1.32	4700	.085
					Average		2690	1.39	4840	.104

Shear Tests

Specimen	h	b	Py	τ_y
A-1	.96	.47	1075	1144
A-2	.98	.47	1015	1102
A-3	.94	.44	1050	1270
A-4	1.02	.46	805	857
		Average		1093

Charpy Impact Tests

Specimen	A	I (ft-lb)
A-1	.447	40
A-2	.413	40
A-3	.424	40
A-4	.47	42
A-5	.437	42
A-6	.472	40
A-7	.48	42
Average	.45	40.8

Impact Energy/Area = 90.5 ft-lb/in^2

Cube Compressive Tests (Unreinforced mortar)

Specimen	σ_c psi
A-1	8870
A-2	8680
A-3	8320
Average	8623

Plate Bending Tests (Thickness = .486)
Deflection Surface at Ultimate Bending Load

	Station				
Spec	1	2	3	4	5
A-1	.0815	.06	.055	.03	.01
A-2	.088	.075	.07	.04	.01
A-3	.085	.05	.045	.035	.03
A-4	.086	.05	.03	.03	.01
A-5	.075	.06	.055	.035	.015
A-6	.088	.09	.065	.035	.01
A-7	.092	.03	.02	0	0
A-8	.066	.08	.06	.02	.015
A-9	.072	.07	.04	.03	0
A-10	.08	.04	.03	.01	.01
A-11	.072	.06	.05	.04	.01
Av.	.0805	.0604	.0473	.0277	.0109

Center Point Deflection Vs. Load

Spec	Load 100	150	200	300	400	583	800	1000	1725
A-1	.01	.0145	.02	.0325	.044	.0815	.2875	.4089	-
A-2	.006	.014	.013	.025	.04	.038	.39	.535	.992
A-3	.005	.008	.014	.021	.035	.085	.256	.366	.834
A-4	.006	.01	.012	.023	.041	.086	.22	.348	.984
A-5	.005	.008	.014	.03	.054	.075	.288	.418	.804
A-6	.007	.011	.01	.018	.030	.088	.368	.502	.976
A-7	.004	.006	.012	.018	.028	.092	.21	.32	.72
A-8	.006	.008	.012	.024	.044	.066	.198	.32	.712
A-9	.005	.008	.016	.031	.048	.072	.304	.424	.814
A-10	.008	.012	.012	.028	.04	.08	.266	.396	1.026
A-11	.004	.007	-	-	-	.072	.334	.484	.964
Aver.	.0066	.00968	.0135	.02505	.0404	.0805	.29	.417	.874

Note:
a) All units in inches, pounds and psi except where noted.
b) Values of E and G are X 10^6.

APPENDIX 1B

Experimental Results: B-Series (Combination 42 mil steel mesh and 17 mil steel fiber reinforced specimens)

Tensile Tests

x, y Direction

Spec	A	P_y	P_u	ϵ_y	ϵ_u	σ_y	E	σ_u	E_p
B-1	.466	315	490	.00018	.00084	675	3.75	1050	.568
B-2	.48	287	475	.00019	.00224	598	3.15	990	.25
B-3	.466	270	450	.00016	.00108	578	3.61	965	.42
B-4	.44	255	450	.00016	.00060	580	3.63	1020	1.0
B-5	.461	280	475	.00018	.00176	608	3.36	1030	.267
				Average		608	3.5	1011	.501
							$x 10^6$		$x 10^6$

45° to x, y Direction

Spec	A	P_y	P_u	ϵ_y	ϵ_u	σ_y	E	σ_u	E_p
B-1	.484	170	350	.0001	.00068	352	3.52	724	.642
B-2	.442	310	310	.0002	-	703	3.52	703	-
B-3	.455	280	310	.00018	.0004	615	3.41	632	.27
B-4	.46	310	320	.00013	.00022	675	3.77	695	.5
B-5	.473	295	-	-	-	617	-	-	-
				Average		594	3.55	701	.47
							$x 10^6$		$x 10^6$

Flexure Tests

x, y Direction

Spec	b	h	P_y	P_u	δ_y	δ_u	σ_y	E	σ_u	E_p
B-1	1.0	.475	75	135	.015	.115	1620	1.32	2910	.157
B-2	1.09	.51	-	165	-	.025	-	-	2840	-
B-3	.9	.49	65	142	.0125	.062	1465	1.39	3200	.413
B-4	.97	.52	100	175	.0175	.197	1855	1.19	3250	.093
B-5	1.04	.52	75	187	.0125	.2	1300	1.16	3250	.12
B-6	1.07	.57	95	205	.0112	.074	1325	1.21	2875	.222
B-7	.91	.57	80	162	.0125	.117	1315	1.08	2670	.132
B-8	.97	.53	75	205	.0125	.113	1340	1.18	3670	.253
				Average			1460	1.22	3090	.198
								$x 10^6$		$x 10^6$

45° to x, y Direction

Spec	b	h	P_y	P_u	δ_y	δ_u	σ_y	E	σ_u	E_p
B-1	.9	.53	75	107	.0175	.0725	1450	.91	2060	.122
B-2	.98	.53	75	135	.0125	.05	1325	1.165	2390	.312
B-3	.9	.53	75	130	.01	.035	1450	1.59	2500	.462
B-4	.94	.51	60	145	.0125	.0475	1200	1.09	2390	.55
				Average			1355	1.19	2460	.362
								$x 10^6$		$x 10^6$

Shear Tests

Specimen	b	h	P_y	λ_y
B-1	.95	.55	990	895
B-2	1.0	.5	1100	1100
B-3	.95	.55	1000	960
B-4	.96	.52	810	812
B-5	.95	.5	1250	1316
B-6	.95	.5	1100	1160
	Average			1040

Charpy Impact Tests

Specimen	b	h	I (ft-lb)	A
B-1	.59	.96	74	.566
B-2	.58	.98	69	.567
B-3	.58	1.01	64	.586
B-4	.53	1.0	44	.53
B-5	.55	.94	49	.513
B-6	.54	.93	46	.502
B-7	.53	1.0	53	.53
B-8	.52	.98	72	.51
	Average		58.9	.538

Impact Energy/Area = 109.5 ft-lb/in^2

Cube Compressive Tests (Unreinforced Mortar)

Specimen	σ_c psi
B-1	8500
B-2	7000
B-3	8500
Average	8000

Plate Bending Tests (Thickness = .53")
Deflection Surface at Ultimate Bending Load

	Station				
Specimen	1	2	3	4	5
B-1	.123	.09	.06	.03	.01
B-2	.087	.07	.05	.0325	.015
B-3	.0885	.085	.07	.0525	.025
B-4	.1105	.085	.065	.025	.015
B-5	.125	.075	.055	.04	.01
B-6	.134	.07	.06	.05	.025
B-7	.157	.09	.06	.04	.03
B-8	.131	.08	.06	.035	.01
B-9	.095	.07	.05	.025	.02
B-10	.104	.06	.04	.035	.02
B-11	.082	.055	.04	.03	.01
B-12	.108	.085	.06	.04	.02
B-13	.085	.06	.045	.04	.01
Average	.11	.075	.055	.0402	.0169

Center Point Deflection Vs. Load

Spec	Load 100	150	200	300	400	500	600	816
B-1	.005	.007	.009	.015	.025	.036	.064	.123
B-2	.004	.008	.01	.015	.025	.034	.049	.087
B-3	.005	.008	.009	.0135	.0235	.0295	.0465	.0885
B-4	.005	.007	.009	.0125	.0185	.0225	.0305	.1105
B-5	.005	.008	.012	.016	.027	.035	.061	.125
B-6	.005	.007	.01	.013	.019	.023	.034	.134
B-7	.006	.009	.012	.016	.029	.037	.069	.157
B-8	.006	.01	.014	.019	.033	.044	.071	.131
B-9	.0055	.008	.011	.016	.03	.035	.049	.095
B-10	.006	.01	.016	.02	.028	.036	.050	.104
B-11	.005	.008	.012	.016	.023	.029	.048	.082
B-12	.006	.008	.012	.016	.024	.032	.054	.108
B-13	.005	.008	.011	.015	.021	.025	.033	.085
Aver.	.00522	.00815	.0113	.0156	.0251	.0322	.0507	.11

Spec	Load 1000	1150
B-1	.594	.894
B-2	.471	.711
B-3	.494	.636
B-4	.387	.601
B-5	.808	.808
B-6	.542	.898
B-7	.602	.762
B-8	.79	.91
B-9	.51	.614
B-10	.59	.83
B-11	.518	.652
B-12	.512	.692
B-13	.291	.737
Aver.	.55	.737

APPENDIX IC

Experimental Results: C-Series (16 mil steel fiber reinforced specimens)

Tensile Tests
All Directions

Spec	b	h	P_y	P_u	ϵ_y	ϵ_u	σ_y	E	σ_u	E_p
C-1	.44	.95	245	300	.00014	.00042	586	4.18	718	.47
C-2	.43	.93	190	247	.00012	.0006	475	3.95	618	.298
C-3	.43	.95	235	295	.00015	.00106	575	3.83	722	.162
C-4	.42	.94	210	295	.00016	.00040	533	3.32	746	.39
C-5	.44	.94	260	300	.00016	.00036	629	3.93	725	.48
C-6	.43	.95	200	385	.00016	.00136	491	3.07	942	.375
C-7	.43	.90	160	215	.00010	.0024	414	4.14	556	.473
				Average			530	3.77	721	.449

Flexure tests

Spec	b	h	P_y	P_u	δ_y	δ_u	σ_y	E	σ_u	E_p
C-1	.87	.49	82	155	.015	.047	1910	1.645	3620	.635
C-2	.9	.45	50	75	.0125	.03	1335	1.385	2000	.492
C-3	.92	.54	80	113	.0135	.027	1450	1.16	2050	.48
C-4	.95	.48	70	105	.0125	.025	1560	1.52	2340	.767
				Average			1560	1.43	2510	.594
								x 10^6		x 10^6

Shear Tests

Specimen	b	h	P_y	λ_y
C-1	.56	.89	820	824
C-2	.5	.91	750	824
C-3	.49	.94	730	792
C-4	.56	.95	830	780
		Average		805

Charpy Impact Tests

Specimen	b	h	I (ft-lb)	A
C-1	.53	.91	80	.482
C-2	.56	1.0	82	.56
C-3	.53	1.0	114	.53
C-4	.47	1.0	98	.47
C-5	.44	1.0	98	.44
C-6	.47	.97	90	.455
C-7	.47	.87	84	.408
	Average		92.5	.478

Impact Energy/Area = 193 ft-lb/in^2

Cube Compressive Tests (Unreinforced Mortar)

Specimen	σ_c (psi)
C-1	8250
C-2	9825
C-3	6000
Average	7920

Plate Bending Tests (Thickness = .513)
Deflection Surface at Ultimate Bending Load

	Station				
Specimen	1	2	3	4	5
C-1	.084	.07	.06	.05	.03
C-2	.096	.09	.08	.06	.03
C-3	.095	.07	.04	.03	.01
C-4	.105	.07	.05	.03	.02
C-5	.1	.07	.06	.03	.01
C-6	.094	.06	.05	.03	.015
C-7	.098	.07	.05	.04	.01
C-8	.112	.06	.05	.035	.03
C-9	.11	.075	.045	.03	.025
C-10	.12	.11	.08	.045	.03
C-11	.128	.075	.06	.04	.03
C-12	.12	.07	.05	.03	.02
Average	.105	.0741	.0562	.0375	.0216

Center Point Deflection vs. Load

	Load						
Spec	100	150	200	300	400	600	780
C-1	.004	.008	.01	.018	.03	.048	.084
C-2	.006	.01	.014	.022	.034	.056	.096
C-3	.005	.008	.01	.016	.025	.041	.095
C-4	.005	.009	.013	.019	.029	.047	.105
C-5	.006	.008	.012	.018	.032	.054	.1
C-6	.006	.01	.014	.02	.032	.05	.094
C-7	.006	.008	.011	.017	.028	.054	.098
C-8	.005	.01	.013	.022	.036	.066	.112
C-9	.008	.012	.018	.028	.041	.07	.11
C-10	.008	.012	.016	.028	-	-	.12
C-11	.008	.011	.015	.024	.04	.066	.128
C-12	.006	.01	.012	.02	.036	.072	.12
Av.	.00608	.00966	.01318	.021	.0330	.0567	.105

APPENDIX ID

Cylinder Test Data (2" x 4" Mortar Reinforced with 3/4" 16 mil steel fibers)

I-Series (Unreinforced Mortar) Area = 3.14 in.^{2}

Specimen	Load 5000	10000	15000	20000	Failure Load
1		.0035	.006	.0085	23,250
2		.0042	.0075	.015	20,650
3	.0025	.005	.008	.014	20,000
4	.0021	.0048	.008	.012	21,000
5	.002	.006	.007	.013	19,250
6	.0018	.004	.007	.011	21,000
7	.002	.0038	.006	.009	26,600
8	.002	.0039	.006	.0095	21,600
9	.0018	.004	.007	.01	23,300
10	.0018	.0038	.0062	.0098	24,400
Average δ	.002	.0043	.00687	.0118	22,105

Lever factor $\delta = \frac{1}{2}$ Def. reading $\sigma_c = 7060$

$$\epsilon = \frac{1}{2}\frac{\delta}{G.L.} = \frac{\delta}{6}$$

Average stress strain curve				
Stress	1590	3190	4780	6370
Strain	.000333	.000716	.001145	.00197

.002 Offset Secant Elastic Modulus

$E = 3.2 \times 10^6$

II-Series (Reinforcement 4.75% fiber by volume) Area = 3.14 in.^{2}

Specimen	5000	10000	15000	20000	25000	Failure Load
1	.002	.0035	.007	.01	.019	29500
2	.0017	.004	.006	.01	.025	25400
3	.0013	.003	.005	.008	.015	27250
4	.0013	.003	.006	.01	.017	29500
5	.0015	.003	.005	.0075	.0105	27600
6	.0019	.004	.0065	.010	.015	28600
7	.0015	.0025	.0044	.0065	.011	27400
8	.0015	.0037	.0065	.00105	.015	29200
9	.0015	.0034	.006	.010	.018	27100
10	.002	.004	.0065	.0090	.015	26200
11	.0016	.003	.0053	.008	.013	27100
12	.0017	.0032	.006	.009	.014	27000
13	.0015	.003	.0053	.0086	.013	27000
14	.0018	.0034	.0058	.008	.014	27500
15	.002	.004	.006	.009	.015	27100
Average δ	.00165	.00338	.00582	.00831	.0153	27500
ϵ	.000275	.000564	.00097	.001385	.00255	
Stress	1590	3190	4780	6370	7970	σ_c = 8775

Secant elastic modulus to .002 offset

$E = 3.83 \times 10^6$

III-Series (Reinforcement 2.37% by volume) Area = 3.14 in.^{2}

Specimen	Load 5000	10000	15000	20000	25000	Failure Load
1	.003	.0058	.0032	.0112	.014	25500
2	.002	.004	.007	.01	.014	29000
3	.003	.0049	.0075	.01	.015	29000
4	.0021	.004	.0067	.0094	.014	26500
5	.0023	.0039	.0065	.009	.016	25400
6	.0028	.0051	.008	.01	.013	25000
7	.003	.0055	.009	.012	-	22400
8	.0025	.0054	.0086	.0125	.018	26000
9	.0032	.0056	.0079	.011	-	24500
10	.0022	.0045	.0078	.011	-	24000
11	.0028	.0052	.009	.012	.017	25600
12	.004	.0072	.01	.013	-	23200
13	.003	.005	.008	.01	.0149	27050
14	.002	.0042	.0065	.0095	-	24000
15	.003	.0055	.008	.011	-	23000
Average δ	.00272	.00505	.0079	.01075	.0151	25300
ϵ	.000454	.000341	.001315	.00179	.00252	
Stress	1590	3190	4730	6370	7970	σ_c = 8060

$E = 3.35 \times 10^6$

APPENDIX II

Finite Element Analysis: Significant Input - Output

Plate Series A

Input

$E_x = 2.91 \times 10^6$
$E_y = 2.91 \times 10^6$
$G = 1.212 \times 10^6$
$\nu = .2$
$E_{px} = .520 \times 10^6$
$E_{py} = .520 \times 10^6$
$E_{p45} = .276 \times 10^6$
$G_p = 0$
$\sigma_{cx} = .830$ kips
$\sigma_{cy} = .830$ kips
$\sigma_{c45} = .598$ kips
$\tau_c = 1.093$ kips
Thickness = .428 in.
Incremental Load = $\dfrac{\text{Elastic Limit Load}}{5}$

Output

	Load(lb)	Center Point Deflection (in)
(Elastic Limit)	76.6	.00514
	91.92	.0066047
	107.24	.00783
	122.56	.009235
	137.88	.010349
	153.2	.011945
	168.52	.013068
	183.84	.014889
	199.16	.016225
	214.48	.017738
	229.8	.019353
	245.12	.020726
	260.44	.021899
	275.76	.023727
	291.08	.025183
	306.4	.0268

Plate Series B

Input

$E_x = 3.5 \times 10^6$
$E_y = 3.5 \times 10^6$
$G = 1.456 \times 10^6$
$\nu = .2$
$E_{px} = .501 \times 10^6$
$E_{py} = .501 \times 10^6$
$E_{p45} = .470 \times 10^6$
$G_p = 0$
$\sigma_{cx} = .608$ kips
$\sigma_{cy} = .608$ kips
$\sigma_{c45} = .594$ kips
$\tau_c = 1.040$ kips
Thickness = .472 in.
Incremental Load = $\dfrac{\text{Elastic Limit Load}}{5}$

Output

Load (lb)	Center Point Deflection (in)
91.36	.00379
109.63	.004736
127.9	.005568
146.17	.0065958
164.44	.0076912
182.71	.008783
200.98	.009822
219.25	.010979
237.52	.012094
255.78	.01326
274.06	.014388
292.33	.015556
310.60	.016671
328.87	.017864
347.14	.018924
365.41	.020035

Plate Series C

Input

$E_x = E_y = 3.77 \times 10^6$

$G = 1.57 \times 10^6$

$E_{0x} = E_{py} = E_{p45} = .449 \times 10^6$

$\sigma_{0x} = \sigma_{0y} = \sigma_{045} = .530$ kips

$\tau_0 = .805$ kips

$t = .455$

$\nu = .2$

$G_p = 0.$

$$\text{Incremental Load} = \frac{\text{Elastic Limit Load}}{5}$$

Output

Load (lb)	Center Point Deflection (in)
76.48	.003287
91.68	.004097
106.88	.004956
122.08	.005866
137.28	.006808
152.48	.00779
167.68	.00832
182.88	.009706
198.08	.01002
213.28	.011513
228.48	.01246
243.68	.01342
258.88	.01434
274.08	.01533
289.28	.01627
304.48	.01714

APPENDIX III

Classical Homogeneous Plate Bending Theory Prediction

A Series

$E = 2.91 \times 10^6$ $e = .45$
$\sigma_y = .330$ kips $c = a/2$
$h = .428$ in. $\alpha = .1265$
$\nu = .2$ $\gamma_1 = -.565$
α, γ_1 from (32) p 165

Combining equation (22) and (18) gives the yield load:

$$P_y = \frac{\sigma_y}{\frac{6}{h^2 4\pi}\left((1+\nu)\log\frac{2a\sin\frac{\pi c}{a}}{\pi e}+1\right)+\frac{\gamma_1}{4\pi}}$$

$$= 77.2 \text{ lb}$$

From equation (16) the maximum deflection occurs at the plate center and is:

$$W_{max} = \frac{\alpha P_y a^2}{E h^3}$$

$$= .0043''$$

B Series

$E = 3.5 \times 10^6$ $e = .45''$
$\sigma_y = .608$ kips $c = a/2$
$h = .472''$ $\alpha = .1265$
$\nu = .2$ $\gamma_1 = -.565$

$$P_y = \frac{608}{2.15\ (4.18)\ -.045} = 68.1\ lb$$

$$W_y = \frac{(68.1)\ (100)\ (.1265)}{3.5 \times 10^6\ (.105)} = .00235''$$

C Series

$E = 3.77 \times 10^6$ $e = .45''$

$\sigma_y = .530$ kips $c = a/2$

$h = .455''$ $\alpha = .1265$

$\nu = .2$ $\gamma_1 = -.565$

$$P_y = \frac{530}{2.31\ (4.18)\ -.045} = 55\ lb.$$

$$W_y = \frac{(55)\ (100)\ (.1265)}{3.77 \times 10^6\ (.0942)} = .00196''$$

thesC4796
Bending of ferro-cement plates.
3 2768 002 10245 1
DUDLEY KNOX LIBRARY